applied sciences

Article

A Novel Rate of Penetration Prediction Model Integrating Log-Derived Geomechanical Properties and Physically Motivated Energy Parameters for Heterogeneous Formations

Ahmed S. Alhalboosi, Musaed N. J. AlAwad and Mohammed A. Khamis *

Department of Petroleum and Natural Gas Engineering, College of Engineering, King Saud University, Riyadh P.O. Box 800, Saudi Arabia; malawwad@ksu.edu.sa (M.N.J.A.)
* Correspondence: mokhamis@ksu.edu.sa

Abstract

Accurate rate of penetration (ROP) prediction in heterogeneous formations remains a key challenge for drilling optimization, as existing empirical models rely on fixed-structure coefficients unable to adapt to rapid lithological transitions. This study presents a novel exponential-form ROP model integrating surface drilling parameters (weight on bit (W), rotary speed (N), torque (T), and standpipe pressure (SPP)), log-derived geomechanical properties (dynamic combined compressibility modulus for carbonates; total porosity for sandstones), and three physically motivated energy parameters: rotational mechanical power per unit bit area (Prot), axial crushing energy (AE/AEs), and hydraulic cleaning efficiency (Hce). Bit wear is quantified through a modified Hareland and Hoberock wear function requiring no laboratory measurements. Parameter selection used combined Pearson and Spearman correlation analysis across 16 candidate variables from a raw dataset of 9375 depth readings for Well A and 4443 for Well B (at 0.25 m intervals). The model was developed using nonlinear least squares regression (Levenberg–Marquardt algorithm) in MATLAB. Validated on two vertical wells penetrating mixed carbonate and clastic sequences in a Middle Eastern offshore field and benchmarked against four classical formulations, the model achieves R^2 = 0.6568–0.6766 across full heterogeneous sections, improving on the best benchmark by margins of 0.36–0.46. Under lithology-specific calibration, R^2 advances to 0.8239–0.9139, with MAPE reducing to 5.71%. The model is limited to two vertical wells in a single field; further field validation is recommended before broader deployment.

Keywords: rate of penetration; geomechanical parameters; dynamic combined modulus; heterogeneous formations; drilling optimization

Academic Editors: Nediljka Gaurina-Međimurec, Borivoje Pašić and Petar Mijić

Received: 3 June 2026
Revised: 14 July 2026
Accepted: 19 July 2026
Published: 23 July 2026

1. Introduction

Rate of penetration (ROP) is defined as the footage of drilling per unit time through rock formation and is usually used as a key factor characterizing the drilling operation efficiency. Therefore, accurate prediction of ROP is fundamental to the drilling optimization and control [1–8].

ROP is arguably the single most important real-time indicator of drilling efficiency and directly governs well construction costs. High ROP is desirable as it accelerates reaching the target with less time and cost; however, too-high ROP may affect the hole geometry and cause poor hole cleaning [9–12]. ROP modeling has always been the primary concern of researchers and companies in the industry since it is directly related to the drilling cost; over the past few decades, many authors have studied the effect of different parameters on the ROP; initially, they focused on creating empirical models based on experience results [13].

ROP is affected by many factors; some of them are controllable, while others are uncontrollable [14]. The controllable drilling factors are the operational drilling parameters that can be changed by the driller from the surface such as revolutions per minute (N), weight on bit (W), the flow rate (Q), and standpipe pressure (SPP), whereas the uncontrollable factors are the ones that cannot be changed because of technological or formation factors, for example, rock strength, pore pressure, mud weight, and wellbore trajectory [15,16]. In heterogeneous formations, where lithology and rock strength change rapidly across short depth intervals, this interaction becomes particularly difficult to capture with a single parameterization.

Over the past seven decades, numerous mathematical and empirical models have been developed to quantify the influence of drilling parameters on ROP. The following paragraphs summarize the most significant contributions.

Graham and Muench [17] introduced the first attempts at optimizing drilling parameters; the authors established an empirical mathematical expression for the bit life and ROP as a function of W, depth, and N. Maurer [18] suggested an equation for roller-cone bits to predict ROP, with the bottom hole assumed to be perfectly cleaned. Bingham [19] proposed a simple and experimental model which is a modification of the Maurer model. It is limited to low W and N; however, it does not consider the depth of drilling. Eckel [20] performed numerous micro-bit experiments, which showed that reducing the overbalance pressure can enhance the efficiency of the formation drillability, thus increasing ROP.

Bourgoyne and Young [21] established one of the most important drilling optimization studies and developed an empirical model to predict the rate of penetration based on several drilling parameters. This model is widely used in the oil industry and is considered the best approach to optimize drilling parameters in real time [22]. The model describes the effect of different drilling parameters on ROP, and they proposed a multiple regression analysis to extract eight unknown parameters using well drilling datasets.

Warren [23] presented a perfect cleaning ROP model for soft formation, and this model relates ROP to W, N, UCS, and bit size. To offer comprehensive information regarding the interaction between rock and the bit, he employed experimental response curves and dimensional experiments. Later, Warren adjusted his model by adding a wear function to reflect the impact of bit wear.

Maidla and Ohara [24] tested a drilling model on offshore drilling data and compared the findings with the Bourgoyne and Young model. Their objective was to be able to select bit, bit bearing, WOB, and drill string rotation to minimize drilling costs. Their finding was that ROP for successive wellbores in the same area could be predicted based on the coefficients calculated from past drilling data, resulting in cost savings. They concluded that the drilling model performance depended on the quality of the data used to conduct the syntheses. They presented isocost and iso-ROP graphs for cost effective drilling activities.

Hareland and Rampersad [25] introduced a model for drag bits that relates UCS, W, N, bit geometry, and bit wear. Motahhari et al. [26] developed a PDC model that considers the wear function and confined compressive strength (CCS) instead of UCS besides N, W, and bit size. Hareland et al. [27] created a new simple model for roller-cone bits and used laboratory data to estimate the UCS.

Deng et al. [28] stated that for a tricone bit, the relation between ROP and N is linear, while the relationship between the ROP and the ratio of WOB and rock dynamic compressive strength is a power of 3/2. They concluded that the error in obtaining the ROP based on the static compressive strength was 45 to 50%, while the average error was around 15% when using the dynamic compressive strength to predict the ROP.

Al-AbdulJabbar et al. [29] introduced a new robust model predicting ROP using both drilling parameters (W, Q, N, T, SPP, UCS) and mud properties (density and viscosity) using 7000 real-time data measurements from carbonate formations, achieving an average absolute percentage error (AAPE) of 5% and correlation coefficient of 0.93 using a formation-clustering approach.

The physics-based models mentioned above use empirical coefficients, which are highly dependent on the lithology and continuously varied due to calibration, such that constraining their functional forms [13]. Soares et al. [30] stated that selection of proper model coefficient bounds is a key factor in the effectiveness of ROP modeling.

A major advancement was introduced by Atashnezhad et al. [31], who developed a cutter–rock interaction-based ROP model derived from single-cutter laboratory experiments and scaled to full-hole drilling conditions. Their approach incorporated the interfacial friction angle and provided a more mechanistic interpretation of PDC bit performance.

Akhtarmanesh et al. [32] developed equations based on a single cutter analysis to calculate the threshold point where the calculated threshold depth of cut and weight on cutter. The model also incorporated a wear function wear to improve prediction accuracy under abrasive conditions.

More recently, Mayibeki [33] proposed a novel physics-based ROP model tailored for hard rock drilling under high-temperature and high-confining pressure environments. Unlike previous models, this formulation integrates a temperature- and pressure-dependent rock strength model into the ROP framework. The model structure relates to W, N, and confined compressive strength (CCS), while accounting for bit geometry, wear, and hydraulic efficiency. Table 1 presents commonly used ROP models and their key limitations, highlighting the gaps addressed in this study.

The preceding paragraphs summarize the most significant individual model contributions. Table 1 provides a comprehensive and critically annotated compilation of all 24 models reviewed, organized to highlight the four persistent structural limitations common to existing formulations: (1) exclusion of key parameters, (2) fixed functional exponents, (3) complex bit geometry requirements, and (4) absence of simultaneous integration of log-derived geomechanical properties with surface drilling data and derived energy parameters. These limitations define the research gap motivating this study.

Indeed, using AI and hybrid models effectively increases the ROP accuracy prediction such as the studies of Jahanbakhshi et al. [34], Ahmed et al. [35], Delavar et al. [36], Mohammadi Behboud et al. [37], Delavar and Ramezanzadeh [38], and Saad et al. [39]; however, these approaches require large training datasets, specialized computational resources, and machine learning expertise. Furthermore, their predictive validity is generally restricted to the geographic area and formation type on which they were trained. For broader field applicability, conventional physics-informed models calibrated with metaheuristic or regression-based optimization techniques remain more practical and transferable [13].

Table 1. Widely cited ROP models and their key limitations.

Author(s)	Model Type	Limitations	Author(s)	Model Type	Limitations
Graham and Muench [17]	Empirical	Restricted to vertical wells and roller-cone bits; excludes rock geomechanical properties, hydraulics, and mud parameters; fixed coefficients limit applicability across formations.	Cunningham and Eenink [40]	Empirical/Analytical	Based on laboratory-scale experiments; assumes perfect cleaning and straight hole; restricted to permeable formations; excludes bit wear, geomechanical parameters, and fluid rheology.
Maurer [18]	Semi-Analytical/Theoretical	Assumes ideal bottomhole cleaning; overestimates ROP under real conditions; valid for tri-cone bits only; ignores depth, chip hold-down, bit wear, hydraulics, and confined rock strength, fixed of input parameters.	Galle and Woods [41]	Empirical/Graphical	Graphical solution only—no closed-form equation; restricted to roller-cone bits; excludes depth, hydraulics, and quantitative geomechanical inputs; cannot be integrated into numerical optimization.
Bingham [19]	Empirical	Assumes perfect cleaning; valid only at low W/N; excludes pore pressure, hydraulics, mud properties, and geomechanical parameters (UCS, CCS); fixed exponent a5 requires empirical calibration per formation.	Eckel [20]	Empirical (Laboratory)	Derived from small-scale microbit experiments; uncertain scaling to field conditions; excludes W, N, rock geomechanical properties, and bit wear; coefficients calibrated under laboratory conditions only.
Bourgoyne and Young [21]	Statistical/Multiple Regression	Regression coefficients are field-specific and require offset well calibration; excludes geomechanical properties (UCS, CCS) and confined rock strength; not applicable to PDC bits or directional wells; fixed log-linear sub-functions cannot adapt to heterogeneous lithology.	Warren [42]	Analytical/Empirical	Assumes perfect bottomhole cleaning; calibrated for soft-formation roller-cone bits only; excludes bit wear, chip hold-down, depth-dependent strength, and hydraulics; empirical constants require field or laboratory calibration.
Walker et al. [43]	Semi-Analytical/Rock Mechanics-Based	Requires triaxial tests and detailed petrophysical data; Mohr–Coulomb constants are lithology-specific and require individual formation calibration; restricted to roller-cone bits; excludes bit wear, cutter geometry, and directional drilling effects.	Warren [23]	Analytical/Empirical	Restricted to roller-cone bits; hole cleaning function requires independent calibration per fluid type; excludes geomechanical parameters beyond compressive strength (no CCS, ductility); fixed constants are formation- and fluid-specific; chip hold-down effect not explicitly modeled.
Winters et al. [44]	Semi-Analytical	Requires triaxial tests and manufacturer bit specifications; each bit style must be individually characterized; complex bit geometry inputs; restricted to roller-cone bits; excludes hydraulics and directional drilling effects; fixed model structure requires full recalibration across rock types.	Maidla and Ohara [24]	Applied Empirical/B&Y Extension	Not a new model formulation—extends B&Y using offset-well coefficient transfer; predictive accuracy depends entirely on the quality and representativeness of historical drilling data; fixed B&Y functional structure inherited; not applicable beyond the calibrated field area.

Table 1. *Cont.*

Author(s)	Model Type	Limitations	Author(s)	Model Type	Limitations
Hareland and Hoberock [45]	Semi-Analytical/Physics-Based (Roller-Cone)	Primarily used in inverted mode to back-calculate rock strength; direct ROP prediction requires known in-situ strength; chip hold-down estimation relies on accurate pore pressure and mud weight; bit geometry requires manufacturer data; restricted to roller-cone bits and near-vertical wells.	Hareland and Rampersad [25]	Semi-Analytical (PDC/Drag Bit)	PDC bits only; cutter wear fraction requires MWD/LWD data or indirect estimation; complex bit geometry inputs (cutter angles, blade count) require manufacturer specifications; formation-specific constants require recalibration; excludes wellbore inclination and hydraulic jetting effects.
Hareland et al. [27]	Physics-Based/Semi-Analytical	Restricted to roller-cone bits; requires manufacturer bit specifications (complex tooth geometry inputs); bit wear estimation uncertain without real-time MWD; excludes hydraulics, fluid rheology, geomechanical parameters beyond UCS/CCS, and directional drilling.	Hareland et al. [46]	Semi-Analytical	Limited to tri-cone bit geometry; inverted-mode accuracy highly sensitive to bit wear estimation errors; requires manufacturer bit data; excludes hydraulics, mud properties, wellbore inclination, and geomechanical parameters beyond UCS; fixed structure requires recalibration across lithologies.
Motahhari et al. [26]	Physics-Based/Semi-Analytical	Requires motor performance curves and PDC bit specifications (complex cutter geometry inputs); formation-specific constants require recalibration; validated for vertical wells only; excludes hydraulic jetting effects and high-temperature downhole conditions.	Deng et al. [28]	Semi-Analytical/Theoretical	Requires dynamic compressive strength (DCS) from dynamic loading tests—significantly more complex than static UCS; static UCS substitution introduces 45–50% error; restricted to tri-cone bits; fixed power-law exponents; excludes bit wear, hydraulics, and geomechanical parameters beyond compressive strength.
Al-AbdulJabbar et al. [29]	Empirical/Multi-Parameter	Fixed equation structure with only two adjustable exponents (a, b) requires nonlinear regression per new field; exclude bit wear; fixed proportionality constant not adaptable to heterogeneous lithology.	Atashnezhad et al. [31]	Physics-Based/Semi-Analytical	Derived from single-cutter lab experiments; uncertain scale-up to full-hole PDC bit; requires complex bit geometry inputs (cutter angles, density) and manufacturer data; interfacial friction angle δ requires lab measurement; excludes CCS, in-situ stress, pore pressure, and confined geomechanical parameters.

Table 1. *Cont.*

Author(s)	Model Type	Limitations	Author(s)	Model Type	Limitations
Akhtarmanesh et al. [32]	Physics-Based/Semi-Analytical	Developed for geothermal hard-rock environments; not validated for conventional oil and gas formations; requires threshold DOC calculation at individual cutter level; complex bit geometry inputs require manufacturer data; cutter abrasion parameters require specialized lab tests; excludes in-situ stress, pore pressure, and wellbore inclination effects.	Mazen et al. [47]	Semi-Analytical (PDC)	Three-index framework requires independent estimation of drillability, cleaning, and wear indices; complex bit geometry inputs require manufacturer data; validated on three Libyan vertical wells only; excludes CCS, tensile strength, in-situ stress; fixed index weighting may not generalize across heterogeneous lithologies.
Sauki et al. [48]	Modified Empirical/Statistical	Validated on North Kuwait carbonates only; accuracy drops in non-carbonate transitions; loss severity must be classified in real time; eliminates B&Y sub-functions f4 and f5, reducing generality; fixed regression coefficients require recalibration for new fields; excludes CCS, ductility, and in-situ geomechanical stress.	Mayibeki [33]	Physics-Based/Semi-Analytical	Tailored for geothermal/hard rock environments; requires temperature- and pressure-dependent strength characterization from specialized laboratory tests; complex bit geometry inputs required; restricted to near-vertical wells; limited to Ph.D.-stage validation—broader peer-reviewed field verification is pending.

Despite decades of ROP modelling development, the models summarized in Table 1 share persistent structural limitations, which can be grouped into four key issues. First, most formulations neglect influential parameters—particularly torque, rock geomechanical strength, and confined compressive strength—relying on fixed coefficients calibrated on specific datasets. Second, fixed exponents prevent adaptation to heterogeneous formations where lithology and rock strength change rapidly with depth. Third, several PDC-specific models require complex bit geometry inputs (cutter count, blade count, back rake angle, nozzle area) that are not routinely accessible in field operations. Fourth, no existing model simultaneously integrates log-derived geomechanical properties with surface drilling data and derived energy parameters in a single framework.

These limitations define the research gap addressed in this study. A practically deployable ROP model must (1) accommodate lithologically heterogeneous intervals without requiring reformulation; (2) incorporate rock geomechanical properties derivable from standard petrophysical logs available in virtually all wells; (3) represent the coupled energy physics of bit-rock interaction through physically motivated derived parameters; and (4) be calibrated and validated on real field data from representative formations. To meet these requirements, this study pursues four specific objectives: (1) to systematically identify the most influential operational, fluid, and geomechanical parameters controlling ROP through Pearson and Spearman correlation analysis across sixteen candidate properties and multiple bit sizes; (2) to develop a novel ROP model integrating surface drilling parameters, log-derived geomechanical properties (dynamic combined modulus for carbonates; total porosity for sandstones), and three newly engineered energy parameters (rotational power Prot, axial energy (AE/AEs), hydraulic cleaning efficiency (Hce)); (3) to benchmark the proposed model against four established formulations across both full well sections and individual lithological intervals; and (4) to quantify the accuracy improvement achievable through lithology-specific calibration in heterogeneous offshore formations. The proposed model is validated on two vertical wells drilled through various lithological sequences in a Middle Eastern offshore field.

2. Methodology

2.1. Well Description and Data Acquisition

This study utilizes data from two vertical wells, designated Well A and Well B, located in a Middle Eastern oil field. Conventional well log data from these wells is integrated with surface drilling parameters to enable ROP prediction. The available well logs include Gamma Ray (GR), Caliper (CALI), Neutron log (TNPH), Density log (RHOB), Compressional Slowness (DTCO), Shear Slowness (DTSM), Photoelectric Factor (PEF), Resistivity, and Temperature. These measurements provide essential inputs for characterizing formation properties and drilling dynamics. The statistical characteristics, including mean, standard deviation, minimum, and maximum values of the processed datasets for Well A and Well B, are detailed in Tables 2 and 3, respectively.

Table 2. Statistical analysis of the dataset of Well-A.

	Min	**Max**	**SD**	**Mean**	**Mode**	**P10**	**P50**	**P90**
TVD (m)	1000	3370	684.26	2185.062		1237.012	2185.062	3133.112
ROP (m/h)	1.9531	92.7	10.774	19.6865	10.1	8.81	17.3605	33.3341
SPP (psi)	1023.6	2539	257.60	1931.58	1820	1647.729	1882.007	2327.383
Q (L/min)	1091.92	3078	571.275	2278.18	1827	1802	1843.33	3014.836
W (ton)	0.1584	18.9	2.8088	7.4848	7.109	4.4112	7	11.6836
T (Ibf-ft)	944.576	21,686	3072.51	9139.270	6130	5938.919	8633.339	13,668.75
N (rpm)	93.752	286	57.9686	198.977	134.1	132	224	257
BS (in)	8.5	12.25	1.8403	10.0156	8.5	8.5	8.5	12.25
GR	0.3953	182	22.6043	36.388	26	15.6433	30.4211	67.938
RHOB (g/cc)	1.3597	2.997	0.1658	2.4654	2.47	2.262	2.4749	2.6668
TNPH	−0.0261	0.795	0.125	0.2058	0.144	0.0696	0.1765	0.3952
CALI (in)	6.0437	24.864	2.335	10.3619	8.25	8.1688	9.7382	12.372
DTSM (us/ft)	62.8027	421.25	28.1831	139.882	132	110.348	135.777	173.435
DTCM (us/ft)	41.0096	167.45	11.8743	73.9865	69.4	60.3851	73.0954	89.1049
PEF	1.6818	9.4128	1.0247	3.8043	4.95	2.3572	3.6478	4.9794
SP (mv)	−58	43.312	24.9514	−1.285	20	−31.375	6.6875	26.1875
DRES (ohm.m)	0.187	1449.5	4.4848	3.6937	2.421	0.7575	2.762	26.5741
TEMP (c)	56.0429	80.112	6.9489	68.0776		58.4499	68.0776	77.7053
Wear	1	0.83	0.042	0.898				

Table 3. Statistical analysis of the dataset of Well-B.

	Min	Max	SD	Mean	Mode	P10	P50	P90
TVD (m)	1945.6	3131.36	351.01	2523.55		2037.25	2523.56	3009.81
ROP (m/h)	0.2256	47.3879	4.9145	9.0257	8.4647	3.3082	8.545	14.2352
SPP (psi)	547	2369.83	391.38	1534.74	1692	1020.93	1617.15	1989.02
Q (L/min)	757	3262.72	636.82	2095.86	1634	1604.01	1813	2986.56
W (ton)	4.255	29.3758	5.1526	16.5555	22.091	9.2008	16.7725	22.7129
T (Ibf-ft)	2030.9	12,962.7	1441.4	8101.54	8699.2	6175.13	8226.27	9890.22
N (rpm)	45.462	219	58.749	115.733	92.318	60	91	202
BS (in)	8.5	12.25	0.7591	8.6706	8.5	8.5	8.5	8.5
GR	20.996	195.958	29.556	59.4231	42	35.2988	49.3492	106.479
RHOB (g/cc)	1.8161	4.6288	0.3915	2.5619	2.56	2.3049	2.51	2.6724
TNPH	−0.0006	0.5949	0.1059	0.17	0.1825	0.045	0.1598	0.3267
CALI (in)	6.1075	15.3001	0.8149	8.7789	8.5	8.3547	8.4609	9.8518
DTSM (us/ft)	84.929	413.701	29.843	139.082	132	111.972	134.072	169.884
DTCM (us/ft)	42.723	146.247	12.728	72.7944	73.6	59.0436	70.8702	88.4387
PEF	1.7417	10	1.5191	4.5487	4.75	2.3551	4.8096	5.1316
SP (mv)	−64.3	49.4532	14.807	−6.8471	−4	−22.73	−6.8351	7.7144
DRES (ohm.m)	0.1266	1319.32	4.7717	3.4283	2.8371	0.6217	2.7186	28.4328
TEMP (C)	51.222	81.2167	8.659	66.2199		54.2224	66.2203	78.2163
Wear	1	0.83	0.033	0.92				

Data quality control was applied in three stages prior to analysis. First, for depth alignment, the raw dataset contained 9375 depth readings for Well A and 4443 for Well B. Because both the drilling operations and the wireline logging were conducted from the exact same surface elevation reference (LMF: Drill Floor: LOG MEASURED FROM = 11.9 m), the datasets were inherently depth-aligned, meaning no depth shifting was required. Second, for outlier handling, extreme ROP values were intentionally retained because, in heterogeneous formations, they represent real physical events (such as hard stringers, fracture zones, and sudden lithological transitions) rather than sensor errors. However, non-productive intervals—specifically connection times (identified by zero WOB and zero ROP for three or more consecutive samples) and reaming intervals—were strictly excluded based on drilling mode flags. Third, for data normalization, all candidate independent variables were subjected to standard Z-score normalization prior to regression modeling to prevent features with large numerical magnitudes from disproportionately dominating the optimization process.

2.2. Rock Geomechanical Calculation

To estimate rock geomechanical properties of drilled wells, IP (Interactive Petrophysics, 2018) software (developed and commercialized by Geoactive Ltd., Westhill, Scotland) was used to estimate geomechanics properties from the available log data. This software can calculate these properties using empirical correlations specifically for each rock type, which gives us much more accurate results. The lithology column of two wells was carried out through an incorporated approach, combining mud logging data and petrophysical well log analysis. Mud logging data descriptions, documented cuttings, gas readings, and lithological features of drilled rock, were analyzed across all well intervals to provide preliminary lithological classifications. To refine and validate these interpretations depth accuracy, neutron-density and sonic-neutron cross plots were used for each section. Based on these analyses, a lithology column was formed, which is essential for geomechanics rock analysis, especially for unconfined compression strength (UCS) and dynamic elastic properties where the IP software uses different equations to estimate it based on lithology type. To validate the accuracy of the calculated geomechanical properties, cross-plots were constructed between log-derived and core-measured values of uniaxial compressive strength (UCS), Poisson's ratio, Young's modulus, and friction angle. The resulting cross-plots demonstrate good agreement between log-derived and core-measured properties, confirming the reliability of the log-based geomechanical characterization. Figure 1 presents selected geomechanical property profiles for Well A. Table 4 shows the statistical summary of calculated geomechanics, petrophysical, and log-derived parameters (Well B).

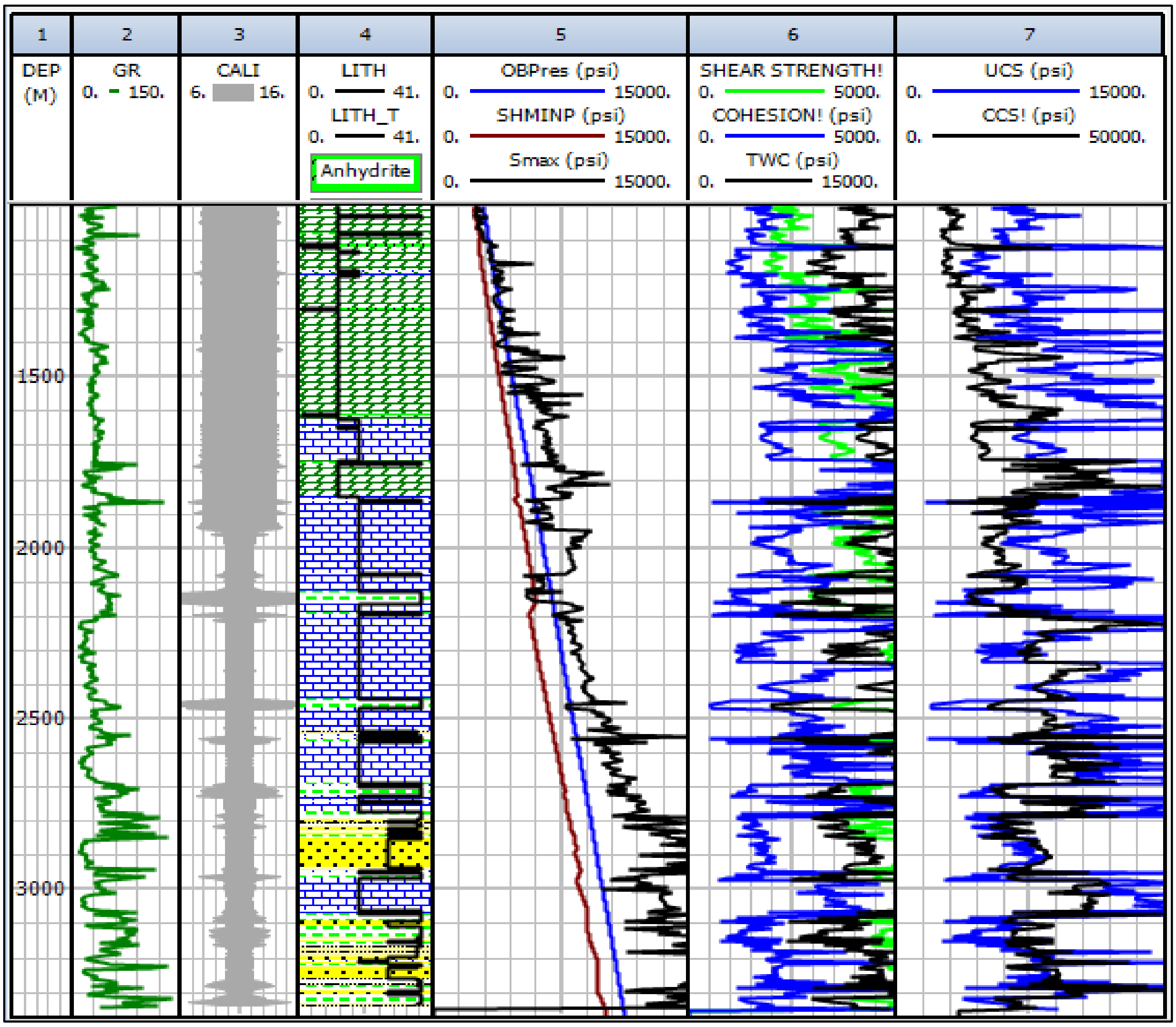

Figure 1. Geomechanical properties of Well A.

https://doi.org/10.3390/app16157383

Table 4. Statistical summary of calculated geomechanics, petrophysical, and log-derived parameters (Well B).

Parameter	Min	Max	SD	Mean	P10	P50	P90
HHP (psi)	76.1292	1139.264	148.88565	365.94338	227.0642	315.442	464.2848
DCM (Mpsi)	1.6236	18.6495	2.5268298	7.1030256	4.16271	6.7738	10.56018
EDYN (Mpsi)	1.5407	16.6235	1.6932293	5.1595275	3.05159	4.8546	7.63536
FA	20.8849	51.1913	6.9888473	37.266410	27.50147	38.1045	45.98736
GDYN (Mpsi)	0.8264	4.23	0.6245575	1.9891227	1.17985	1.87835	2.91769
KDYN (Mpsi)	0.22	13.9082	1.7997971	4.4508623	2.4797	4.3047	6.66537
OBP (Psi)	5878.99	10139.83	1201.4211	8059.5397	6397.305	8056.38	9712.2909
PR	0.1108	0.4624	0.0365845	0.3020366	0.25192	0.3077	0.33649
TWC (Psi)	5300.07	48,426.72	4793.4981	15,752.144	10,066.07	15,053.7	22,428.608
UCS (Psi)	1537.12	81,533.26	6003.2393	11,036.163	4738.813	9595.83	19,328.154
CCS (Psi)	2805.23	87,677.41	7684.1140	19,507.317	10,159.02	18,858.2	30,075.200
COHESION (Psi)	418.288	22,907.03	1570.9485	2992.2725	1438.796	2610.79	5187.5382
SHMINP (Psi)	4888.45	9278.285	1123.4837	7059.0679	5402.454	7106.47	8397.8090
SHMMAX (Psi)	5149.79	23,437.04	2415.4375	9548.5645	6735.701	9090.46	13,132.931
PP (Psi)	1165.19	7211.904	1172.6488	4539.4375	3147.727	4276.53	6275.483
Differ. Press (Psi)	−2419.9	862.115	748.51878	−203.798	−1107.5	−144	810.7331
SHEAR STRENGTH (Psi)	473.433	23,010.5	1600.2912	3160.0564	1538.72	2769.4	5402.522
Dynamic Bulk Compressibility (µsip)	0.1005	0.877	0.1290877	0.2666808	0.1501	0.2317	0.40348
BI	0.043	0.6	0.11	0.33	0.24741	0.323	0.3935
VCL	0	1	0.62	0.11	0.40	0	0.6
PHIT	0.0001	0.2874	0.0749038	0.1079059	0.02044	0.1026	0.21996

2.3. Development of the New ROP Model

ROP is governed by a multitude of interacting parameters, broadly categorized as controllable (e.g., weight on bit, rotary speed) and uncontrollable (e.g., formation lithology, pore pressure). A parameter that strongly promotes ROP in one lithological interval may exert the opposite effect at a shallower or deeper interval where lithology, rock strength, or bit condition has changed.

The relationships between these variables and ROP are highly interdependent and rarely linear. To evaluate these complex relationships, both Pearson and Spearman correlation coefficients were computed between ROP and the full set of available operational parameters, drilling fluid properties, rock geomechanical properties, and petrophysical log measurements. Using both methods together was a deliberate choice: Pearson captures linear relationships, while Spearman captures monotonic but nonlinear associations—and in real drilling data, most parameter–ROP relationships are not strictly linear. Relying on Pearson alone would have caused several important parameters to be underweighted or dismissed. The study therefore systematically isolates and selects the features that exert the most significant statistical impact on drilling performance.

The correlation results of the tested parameters show the complex nature of the relationship between ROP and influencing parameters. As shown in Figures 2–7, the degree of correlation varies throughout the well depending on lithology type, bit size section, bit design, and the interaction between parameters. The Pearson and Spearman correlation coefficients show different degrees of correlation, where the Spearman correlation shows stronger correlation compared to Pearson, reflecting the nonlinear relationship between drilling parameters and ROP. The bit size also influences this difference in correlation.

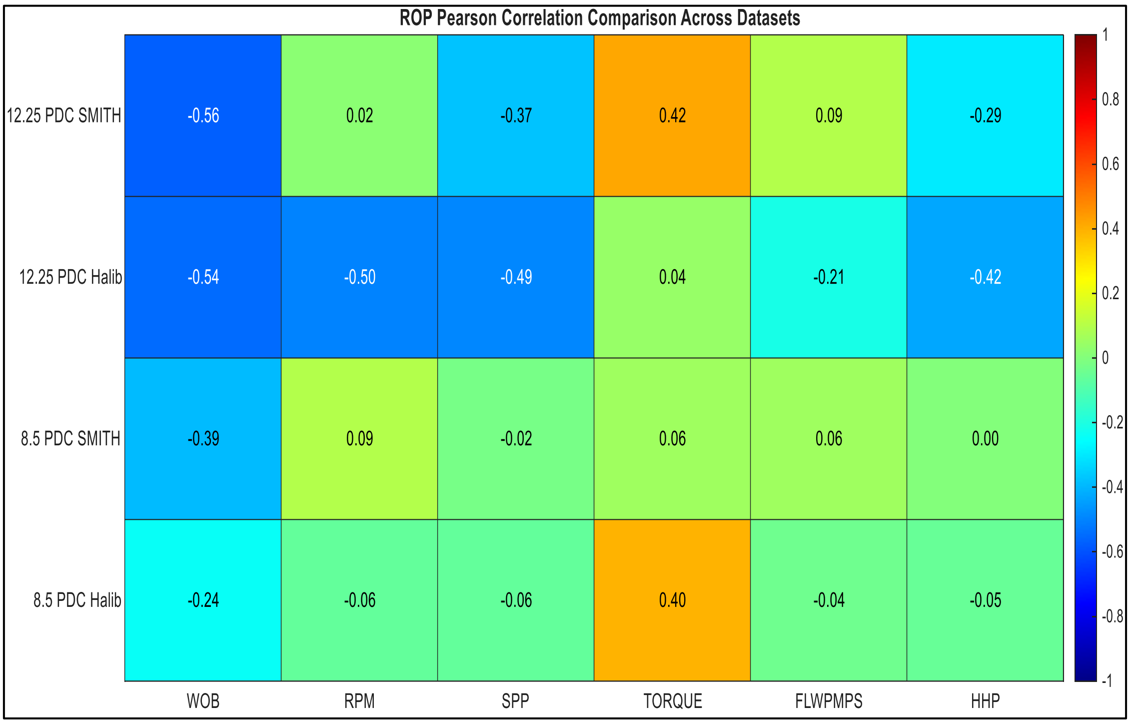

Figure 2. Pearson correlation matrix (heatmap) of ROP versus drilling parameters for different PDC.

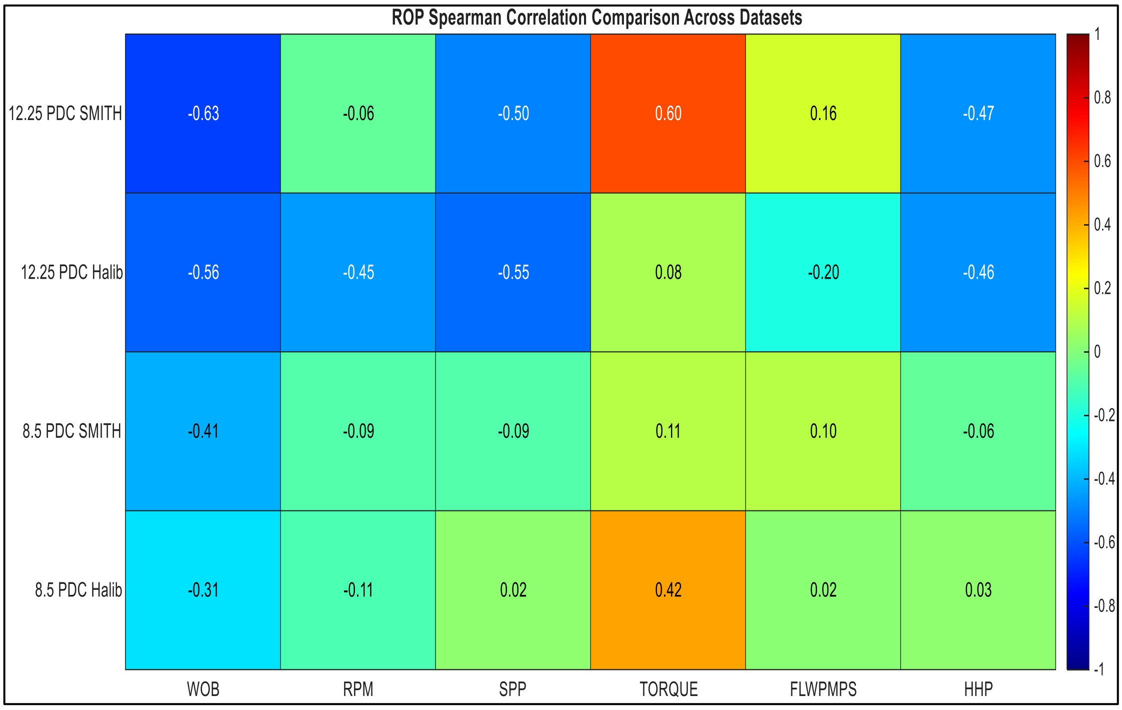

Figure 3. Spearman correlation matrix (heatmap) of ROP versus drilling parameters for different PDC.

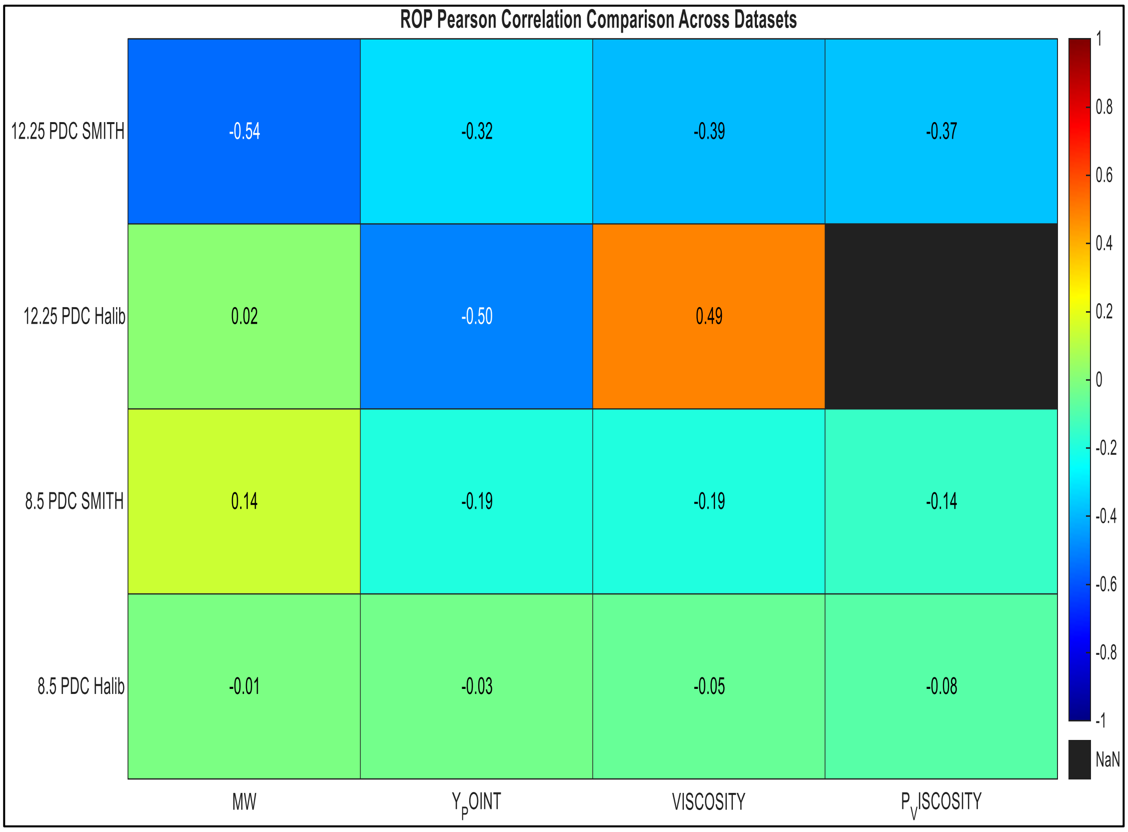

Figure 4. Pearson correlation matrix of ROP and drilling fluid parameters for PDC bits.

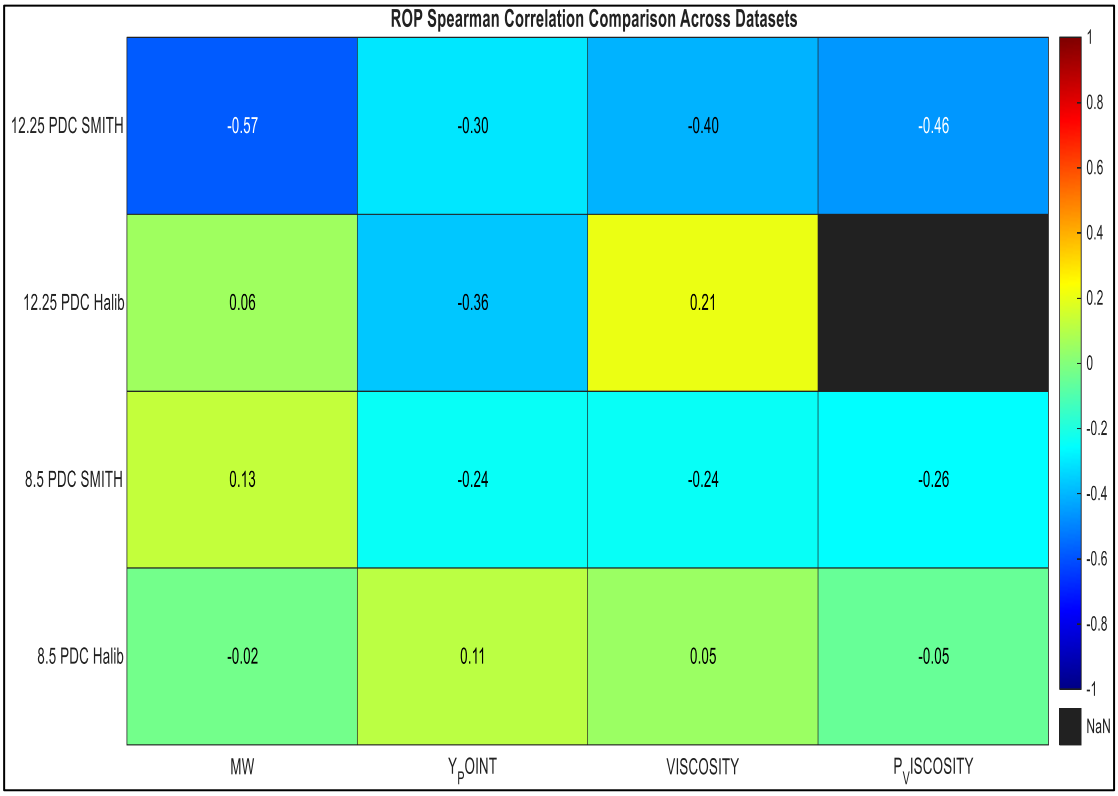

Figure 5. Spearman correlation matrix of ROP and drilling fluid parameters for PDC bits.

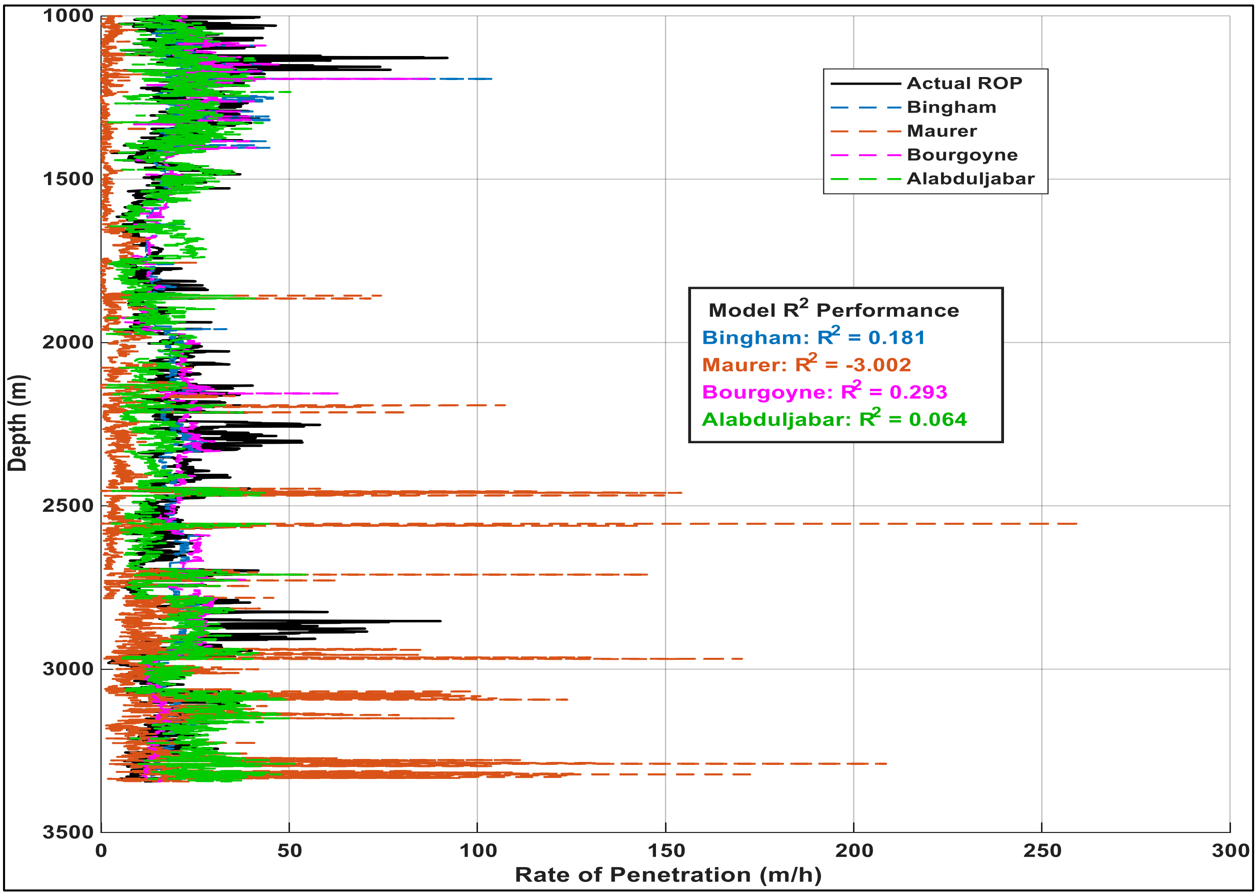

Figure 6. Existing ROP models: measured vs. predicted ROP with depth—(Well A—full section).

The statistical significance of all selected parameters was confirmed through *p*-value analysis of the Pearson and Spearman correlation matrices. All selected parameters exhibit highly significant relationships with ROP, with *p*-values strictly below the $p < 0.01$ threshold. Representative *p*-values include Prot (Pearson $p = 1.15 \times 10^{-58}$), AE (Pearson $p = 5.19 \times 10^{-18}$), W (Pearson $p < 0.001$), N (Pearson $p = 7.62 \times 10^{-30}$), and DCM (Pearson $p < 0.001$). Regarding multicollinearity, Variance Inflation Factor (VIF) analysis was performed on the selected predictors. The computed VIF values are W = 2.31, T = 4.72, N = 18.98, Prot = 13.41, AE = 5.56, and DCM = 2.52. The elevated VIF values for N, Prot, and AE are a direct mathematical consequence of the physics-based feature engineering methodology (whose explicit mathematical formulations are developed in Section 3.1): because Prot and AE are composite variables derived from raw operational sensors (W, N, T), structural multicollinearity is completely expected and physically intentional. While traditional linear regression models suffer when VIF > 5, the proposed ROP framework employs a robust exponential structure where retaining these mathematically correlated terms is essential: the derived parameters (Prot, AE) capture coupled thermomechanical mechanisms (rotational mechanical power per unit bit area, axial crushing energy) that the raw surface sensors alone fail to represent under heterogeneous rock conditions. Therefore, this structural multicollinearity is an intended feature of the physical model design rather than a statistical flaw.

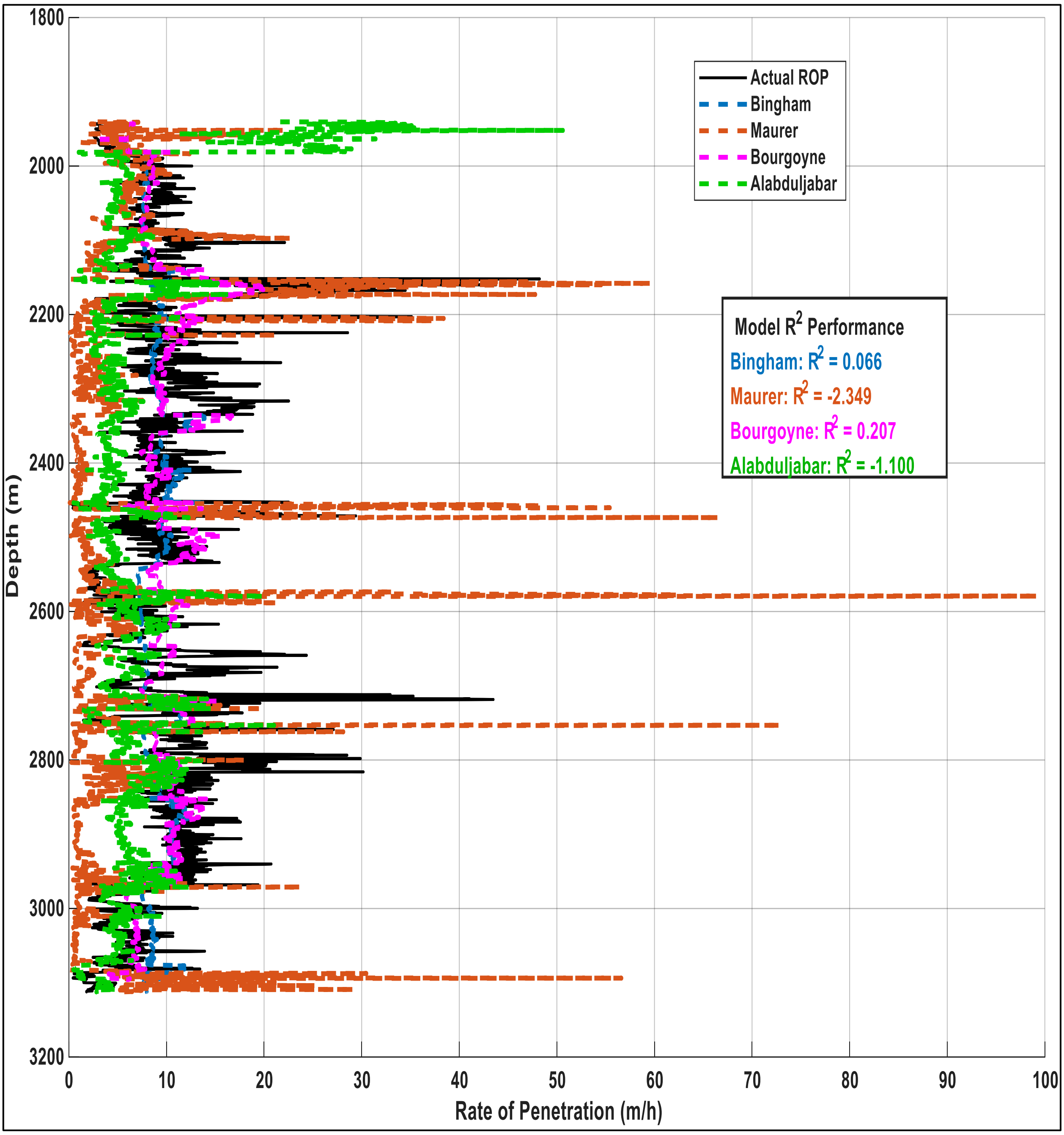

Figure 7. Existing ROP models performance: measured vs. predicted ROP with depth—(Well B—full section).

For operational parameters (Figures 2 and 3), the most influential parameters affecting ROP, which are already considered in previous models, are W, T and N. These show different degrees of correlation—from high to weak—and different signs, reflecting the efficiency of drilling operations and the degree of drilling parameter management and optimization. The fluid hydraulics parameters appear with different degrees of correlation; SPP is selected among them as it shows the highest correlation across different scenarios.

For drilling fluid properties (Figures 4 and 5), the most influential fluid parameters affecting ROP are mud weight, which shows a strong negative correlation particularly for the 12.15-inch bit size and was therefore selected as the primary fluid property parameter. Other fluid parameters show varying degrees of correlation across different bit manufacturers and bit sizes; mud viscosity was selected as a secondary parameter owing to its marginally higher correlation with ROP compared with yield point and plastic viscosity.

For geomechanical rock properties, Alhalboosi et al. [49] systematically evaluated the correlation between sixteen geomechanical parameters and ROP across different lithologies, bit manufacturers, and bit sizes. Their findings demonstrated that confined compressive strength (CCS), shear strength, and dynamic combined modulus (DCM) exhibited the highest correlations with ROP. Furthermore, by modifying the Al-AbdulJabbar et al. [29] empirical model to independently test each of the sixteen parameters, they confirmed that DCM achieved the highest predictive accuracy compared to all other geomechanical inputs.

Model development also uses feature engineering techniques to create new parameters that improve ROP predictions. These parameters are built based on the operational parameters, geomechanical properties, and drilling fluid properties that reflect the interaction between these parameters during the drilling process. A MATLAB code was also developed to examine the mathematical relationships between all selected parameters and ROP, including power law, exponential, and square root functional forms.

To estimate bit wear, most existing models require detailed bit specification data and laboratory-derived rock abrasivity indices that are frequently unavailable in field operations. To overcome this limitation, a novel bit wear equation was developed through modification of the Hareland and Hoberock [45] model, eliminating dependency on unavailable parameters by relying solely on operational inputs (W, N, T) and the dynamic combined modulus (DCM) derived from standard wireline logs. The incremental bit wear (ΔBG) and wear function (W_f) were calculated using Equations (1) and (2), respectively. Validation against the original Hareland and Hoberock [45] model using Run 1 data confirmed comparable predictive performance, with the proposed model achieving slightly superior Pearson and Spearman correlations (-0.5717 and -0.6384, respectively) relative to the Hareland and Hoberock [45] model (-0.5577 and -0.6399). To rigorously evaluate the proposed bit wear function (W_f), the dolomite interval (1000–1758 m) of Well A was selected as a controlled benchmark against the Hareland and Hoberock [45] model. Because rapid lithological transitions in interbedded formations make formation abrasiveness calculations difficult, the uniform mineralogy of this clean dolomite interval allowed for direct, unconfounded isolation of bit wear mechanics. Verifying superior accuracy in this controlled baseline justified applying the model across broader, heterogeneous field sections. The proposed model was therefore selected as the bit wear estimation framework for this study, offering equivalent accuracy while requiring no laboratory measurements or core testing, making it particularly suitable for data-limited field environments.

The empirical coefficient hc was calibrated using a deterministic reverse-engineering approach for each bit run in Well A by equating the cumulative theoretical wear to the IADC dull grade recorded in post-run bit final reports. The calibrated hc values are as follows: Run 1 (1000–1758 m) = 1.350664×10^{-16}; Run 2 (1758–2400 m) = 1.202085×10^{-16}; Run 3 (2400–2900 m) = 1.147194×10^{-16}; Run 4 (2900–3370 m) = 1.510370×10^{-16}. Predicted final wear matched IADC records with 0.00% absolute error across all four runs, confirming that the calibration procedure successfully anchors the theoretical model to physical wear observations. A head-to-head comparison against the Hareland [46] model on Run 1 confirmed slightly superior Pearson correlation (-0.5717 vs. -0.5577) and lower RMSE (9.521 vs. 9.631 m/h), while requiring no laboratory rock abrasivity indices.

In Equations (1) and (2), the parameters are defined as follows: ΔBG is the incremental bit wear accumulated over depth step i (dimensionless, on the 0–8 IADC scale where 0 = new bit and 8 = completely worn); hc is a dimensionless empirical calibration coefficient that is field- and bit-specific, solved analytically to equate cumulative theoretical wear to the IADC dull grade recorded in post-run bit reports; W is weight on bit (kN); N is rotary speed (rev/min); T is surface torque (N.m); DCM is the dynamic combined compressibility modulus at depth step i (MPa); n is the number of depth steps in the bit run; and Wf is the dimensionless wear function representing the fractional drilling effectiveness of the bit (Wf = 1 for a new bit; Wf → 0 for a fully worn bit). The constants a and b follow the Hareland and Hoberock [45] original formulation, with values a = 0.3 and b = 0.5 as adopted in this implementation; the coefficient hc absorbs all field-specific scaling.

$$\Delta BG = h_c \sum_{i=1}^{n} W_i N_i T_i DCM_i \tag{1}$$

$$W_f = 1 - a\left(\frac{BG}{8}\right)^b \tag{2}$$

2.4. Testing of Widely Used ROP Models

Several ROP models have been developed in recent decades, as reviewed in the previous section. In this study, four widely cited models—Maurer [18], Bingham [19], Bourgoyne and Young [21], and Al-AbdulJabbar et al. [29]—are evaluated as benchmark formulations against the proposed model. The exact mathematical functional forms of all four benchmark models are detailed in their respective subsections below (Equations (3)–(14)), while their key structural assumptions and physical limitations are synthesized in Table 1. To ensure a rigorous and direct comparison, these functional forms were implemented exactly as published, with their empirical coefficients estimated via nonlinear least squares regression using the identical datasets applied to the proposed model.

2.4.1. Maurer Model

In 1962, Maurer [18] stated that ROP can be calculated as a function of W, N, drillability strength of the rock (UCS), bit diameter (BS), and the drillability constant (K); the equation is based on a 'perfect cleaning' condition where all of the rock debris has been removed, and Maurer's model is described by Equation (3), as follows.

$$ROP = K\frac{NW^2}{BS^2 UCS^2} \tag{3}$$

2.4.2. Bingham Model

Bingham [19] suggested a model that predicted ROP by considering it as simply function of rotary speed, weight on bit, and bit diameter. Bingham's model is shown in Equation (4):

$$ROP = K\left(\frac{W}{BS}\right)^x N \tag{4}$$

2.4.3. Bourgoyne and Young Model

The authors developed a mathematical model [21] that simplified the rotary drilling process into one single model. The model expresses ROP as a product of eight sub-functions, each representing a specific drilling variable or formation effect. The model is mathematically given by Equation (5):

$$ROP = (f_1) \times (f_2) \times (f_3) \ldots. \times (f_8) \tag{5}$$

In which

$$f_1 = e^{2303a_1} \tag{6}$$

$$f_2 = e^{2303a_2}(10{,}000 - D) \tag{7}$$

$$f_3 = e^{2303 a_3 TVD^{0.69}\left(g_p - 9\right)} \tag{8}$$

$$f_4 = e^{2303 a_4 TVD(g_p - ECD)} \tag{9}$$

$$f_5 = \left[\frac{\left(\frac{W}{BS}\right) - \left(\frac{W}{BS}\right)_t}{4 - \left(\frac{W}{BS}\right)_t} \right]^{a5} \tag{10}$$

$$f_6 = \left(\frac{N}{60}\right)^{a6} \tag{11}$$

$$f_7 = e^{-a_7 h} \tag{12}$$

$$f_8 = \left(\frac{F_j}{1000}\right)^{a8} \tag{13}$$

where TVD shows the true vertical depth (ft), D is depth (ft), g_p is the pore pressure gradient (lbm/gal), ECD expresses the equivalent circulating density (lbf/gal), $(W/BS)_t$ shows the threshold bit weight per inch of bit diameter at which the bit begins to drill (lbf/in), h is bit tooth dullness, and F_j is the jet impact force (lbf).

2.4.4. Al-AbdulJabbar Model

Al-AbdulJabbar et al. [29] used data from carbonate reservoirs in the Middle East to build this empirical model. It combines a comprehensive set of drilling parameters with mud properties and rock strength, which makes it well suited to this study as it represents the interaction of all these properties for the evaluation of which rock geomechanical parameter most effectively predicts ROP. Their model is given by Equation (14). The original formulation employs fixed exponents taken from the authors' calibration dataset:

$$ROP = \frac{16.96(\ W^a \times N\ \times T\ \times SPP \times\ Q)}{BS^2 \times UCS^b \times \rho \times PV} \tag{14}$$

where a and b are model coefficients and will be calculated by nonlinear regression (the authors proposed 0.85 and 1.16, respectively, for the values of these parameters); T is torque (klbf-ft); Q is flow rate (gpm); PV is plastic viscosity (cp); SPP is standpipe pressure (psi); and ρ is the mud density (pcf).

The coefficients of all evaluated models, as well as assessment of model performance, were computed using special MATLAB codes (MATLAB Version 2025b).

Custom-developed MATLAB code (MATLAB Version 2025b) was implemented to ensure consistent assessment of model performance and accurate calculation of the model coefficients. To prevent input features with large numerical magnitudes (such as standpipe pressure and rotary speed) from disproportionately dominating the optimization process, all candidate independent variables were subjected to standard Z-score normalization prior to regression modeling. Following standardization, the model coefficients (β) were iteratively refined using the nonlinear least-squares Levenberg–Marquardt algorithm. The optimization procedure was initialized with preliminary guesses derived from a linearized log-transformation of the exponential equation, iteratively minimizing the residual sum of squares until achieving a strict convergence tolerance limit of 10^{-6}.

3. Results and Discussion

3.1. Model Development and Parameter Selection

Based on the findings from the correlation analysis and the performance evaluation of existing models, a new rate of penetration model was developed. Drawing on the correlation analysis and feature engineering conducted in earlier stages, nine key parameters were selected as independent variables for the ROP prediction model. These parameters comprehensively represent the operational, hydraulic, and geological properties of the drilling process.

Using both Pearson and Spearman correlation techniques, the parameters that exhibited the strongest correlations with ROP—namely, weight on bit (W), torque (T), rotary speed (N), total porosity (PHIT), and dynamic compressibility modulus (DCM)—were selected for inclusion in the new ROP model. The proposed formulation integrates these key parameters while accounting for the nonlinear relationships observed in the data.

In contrast, based on feature engineering techniques, three additional parameters were derived that improved ROP prediction accuracy (see Table 5). The first derived parameter is mechanical power transmitted through drill pipe rotation over the cross-sectional area of the bit, as shown in Equation (15). The second parameter represents the interaction between weight on bit and rotary speed with dynamic strength through over the cross-sectional area of the bit (Equation (16)). For sandstone, DCM was replaced by PHIT in the parameter AEs (Equation (17)). This substitution is physically justified in sandstone formations, as porosity is the dominant control on rock mechanical strength, as established by Allawi et al. [50]. They demonstrated through first-principal derivation that unconfined compressive strength (UCS) in sandstone reservoirs is expressible as a porosity-only function, with validation against 75 Zubair formation core samples yielding $R^2 = 0.9355$. Since geomechanical parameters like DCM reduce to porosity-dependent expressions in sandstones, PHIT captures equivalent mechanical information while being more directly available from standard petrophysical interpretation, and the third parameter was adapted from the Bourgoyne and Young ROP model to represent bit hydraulics and cleaning efficiency. In this formulation, standpipe pressure (SPP) was substituted instead of flow rate (q) due to its stronger correlation with ROP observed in the earlier analysis, and it is expressed in Equation (18).

Table 5. Coefficient of determination (R^2) for the new ROP model configurations using original and derived parameter combinations.

Model Version	Predictors	R2
Independent Sensors Only	W, T, N, BS and others (no calculated terms)	0.5238
W/BS Configuration	W, BS, T, N, and others (removed AE)	0.6275
AE Configuration	AE, T, N, and others (removed W/BS)	0.6361
AE Addition	W, T, N, BS and others + AE	0.5417
Pure Energy	AE, P_{rot}, H_{ce} + WEAR only	0.20
All Parameters	All Parameters combined	0.6568

The nozzle diameter (dn) was obtained from bit run final reports provided by the bit manufacturers for each PDC bit run in both wells. Values were held constant within each bit run (as dn is a fixed bit specification) and updated at bit change boundaries. The nozzle diameter varied between bit runs due to differing nozzle configurations for the 8.5-inch and 12.25-inch bit sections used across both wells.

Selection between the carbonate axial crushing energy formulation (Equation (16), utilizing DCM) and the sandstone formulation (Equation (17), utilizing PHIT) is governed by the section lithology established in Section 2.2. Specifically, carbonate classifications (limestone, dolomite, marly limestone, and anhydrite) strictly apply Equation (16), whereas clastic classifications (sandstones) apply Equation (17). This structural transition is driven by statistical correlation analysis against measured ROP; in carbonate sequences, DCM exhibited the highest correlation with ROP, accurately capturing brittle rock stiffness under axial loading. Conversely, in clastic formations, PHIT yielded the highest correlation, reflecting that pore collapse and intergranular crushing dominate drilling penetration. This substitution was empirically validated during model evaluation: applying DCM in sandstone intervals resulted in a plateaued predictive accuracy of $R^2 \approx 0.70$, whereas substituting PHIT elevated model performance to $R^2 > 0.85$. Furthermore, the reciprocal test—applying PHIT in carbonate intervals—demonstrated a measurable decline in predictive capability relative to DCM, thereby confirming the mechanistic necessity and lithology-specific optimality of each formulation.

$$P_{rot} = \frac{2\pi * N * T}{60 * \frac{\pi}{4} BS^2} \tag{15}$$

$$AE = \frac{W * N}{\frac{\pi}{4} BS^2 * DCM} \tag{16}$$

$$AEs = \frac{W * N * PHIT}{\frac{\pi}{4} BS^2} \tag{17}$$

$$H_{ce} = \frac{\rho * SPP}{\mu * d_n} \tag{18}$$

Overburden pressure (OBP) was included as an additional parameter based on its consistent moderate correlation with ROP across both wells and both Pearson and Spearman analyses (Figures 6 and 7). As drilling depth increases, overburden pressure directly influences the effective confining stress on the formation, which affects the rock failure mechanism and thus the achievable penetration rate. OBP is readily calculated from the bulk density log via numerical integration with depth and requires no additional measurements beyond those already used for DCM calculation.

The mechanical power transmitted to the formation follows from rotational mechanics: $P_{mech} = T \cdot \omega$, where $\omega = 2\pi N/60$. $P_{mech} = 2\pi NT/60$ is then substituted. Normalizing by the bit cross-sectional area = $\pi BS^2/4$ directly yields Equation (15). This represents the intensity of rotational mechanical energy delivered to the rock face per unit area per unit time, capturing the coupled effect of torque and rotary speed normalized for bit size.

To dreive AE and AEs' axial crushing energy per unit bit area, we establish that the applied axial stress at the bit face is $\sigma_{axial} = 4W/(\pi BS^2)$. Incorporating rotational speed (N) to account for continuous dynamic cutter engagement and dividing by the formation's resistance to axial crushing gives the normalized dynamic crushing energy flux. For carbonates, the DCM represents depth-resolved rock stiffness; because higher stiffness inversely resists penetration, placing DCM in the denominator yields Equation (16). Conversely, for sandstones, pore collapse and grain crushing dominate the drilling response, making PHIT a more mechanistically appropriate proxy. Because higher porosity directly promotes clastic failure, acting as a direct multiplier yields Equation (17).

The hydraulic energy available for cuttings' removal is proportional to standpipe pressure (SPP) and mud density (ρ), which govern the momentum flux of the mud jet. This driving force is opposed by viscous resistance (plastic viscosity μ) and distributed across the nozzle exit restriction area (proportional to dn), yielding Equation (18). Higher Hce indicates more effective cuttings removal, maintaining a clean cutting surface and directly supporting higher ROP.

The ROP model development involved evaluating different combinations of parameters through an iterative process. This examination considered the use of original sensor measurements, derived parameters, and combinations of both.

Multiple model configurations were tested to understand the contribution of different parameter groups. Table 5 summarizes the performance of each configuration based on the coefficient of determination (R^2).

The development process of the new ROP model, as summarized in Table 5, demonstrates that while the derived energy parameters (P_rot and AE) are highly predictive, they must be utilized alongside their original surface drilling components rather than in isolation. For instance, when only the derived parameters (P_rot and AE) were used, excluding the original operational measurements (W, T, N), the model achieved an R^2 of only 0.20. This confirms that derived parameters alone fail to capture crucial physical information about the drilling process. Specifically, high torque at a low rotary speed represents a fundamentally different rock-breaking mechanism compared to low torque at a high rotary speed; yet both scenarios could yield similar Prot values. Retaining the original sensors alongside the derived terms preserves this critical mechanical context.

To clarify the composition of the "All Parameters" configuration (R^2 = 0.6568), this model incorporates all nine primary input variables, W, N, T, SPP, OBP, DCM (or PHIT for sandstones), Prot, AE (or AEs), and H_{ce}, together with the bit wear function W_f. This yields exactly 10 model terms, including the intercept β_0.

By integrating these components, a critical finding of the model development process is that the addition of log-derived geomechanical properties and the derived energy parameters (P_{rot} and AE) contributes an absolute R^2 improvement of 0.133 beyond surface sensor measurements alone (increasing from 0.5238 to 0.6568). This confirms that these advanced parameters carry vital predictive information regarding rock–bit interactions that is not present in raw surface drilling measurements.

Based on the preceding analysis, the final ROP model for heterogeneous formations is given by Equation (19):

$$ROP = exp\left(\beta + \beta_1(\ln W) + \beta_2\sqrt{T} + \beta_3(\ln N) + \beta_4(\ln DCM) + \beta_5 OBP + \beta_6\sqrt{P_{rot}} + \beta_7 AE + \beta_8 H_{ce} + \beta_9 W_f\right) \quad (19)$$

This model achieves high accuracy when applied to individual formations, particularly in dolomite and limestone intervals.

For sandstone formations, the model was modified by replacing DCM with PHIT to improve predictive performance, resulting in Equation (20):

$$ROP = exp\left(\beta + \beta_1(\ln W) + \beta_2\sqrt{T} + \beta_3(\ln N) + \beta_4(\ln PHIT) + \beta_5 OBP + \beta_6\sqrt{P_{rot}} + \beta_7 AE + \beta_8 H_{ce} + \beta_9 W_f\right) \quad (20)$$

3.2. Model Verification for the Full Well Lithology Sections

The proposed ROP model was first validated across entire well sections for Wells A and B to establish its baseline performance in heterogeneous formations. For comparison, the existing ROP models were also applied to the same two wells.

The results confirm that the new model achieves the best predictive performance across both wells. The Maurer model failed to predict ROP accurately in full-section mode because its fixed power law exponents (W^2, N, UCS^2) cannot adapt to the continuously varying lithology, pressure, and hydraulic conditions encountered during real drilling. As depth increases, bit-formation interaction changes character from aggressive cutting in soft carbonates to grinding in hard dolomite, thus invalidating fixed functional forms.

The Bingham model produces only a central trend through measured ROP data, providing no ability to track ROP variation with depth; it effectively represents a formation-averaged constant rather than a dynamic predictor.

The Bourgoyne and Young model performs best among the benchmarks for full sections, as its eight sub-functions accommodate more physical mechanisms; however, its exclusion of formation geomechanical strength limits its performance in lithologically diverse intervals.

The Al-AbdulJabbar model, although calibrated on similar Middle East carbonate formation, failed to generalize across the mixed carbonate–clastic sequences of these wells, confirming that formation-specific fixed exponents cannot represent cross-lithology drilling behavior.

The constants of all evaluated models for both wells are presented in Table 6. Figures 6 and 7 show the performance of the tested models with depth, demonstrating that these models are unable to predict ROP accurately in heterogeneous formations; the agreement between predicted and measured ROP is particularly weak for Well B, while the new model achieves good agreement with actual ROP.

Table 6. Calibrated model constants for both wells.

Model	Constant	Well A	Well B
Maurer	K	2.4309	0.7948
Bingham	K	47.8179	830.7095
	a	−0.5088	−0.3507
	b	0.5190	−0.3991
Al-AbdulJabbar	a	0.1396	0.1000
	b	0.6693	0.6071
Bourgoyne and Young	a1	−0.332050	0.388601
	a2	1.420142×10^{-4}	3.929264×10^{-4}
	a3	5.707191×10^{-4}	1.550878×10^{-3}
	a4	-3.276832×10^{-5}	-8.427491×10^{-5}
	a5	−0.387843	−0.515036
	a6	1.983718	−0.434952
	a7	−0.642054	−0.770162
	a8	1.019746	0.362816

Three primary mechanistic reasons explain the underperformance of the Al-AbdulJabbar et al. model despite being developed in a similar Middle Eastern carbonate context: (1) the model relies on fixed power law exponents calibrated to specific carbonate data clusters, rendering it unable to dynamically adapt when drilling through rapidly interbedded sequences of dolomite, limestone, and sandstone within the same bit run; (2) while unconfined compressive strength (UCS) serves as a conventional static rock strength indicator, the dynamic combined compressibility modulus (DCM) employed in this study provides a superior representation of in situ elastic stiffness and brittle rock failure mechanics under continuous dynamic bit engagement; and (3) the original Al-AbdulJabbar methodology relies heavily on a pre-drilling formation-clustering workflow. Because re-clustering was not applied to our continuous field data, the model was constrained to a single static coefficient set across all heterogeneous intervals, severely restricting its predictive capability.

Tables 6–8 present the performance metrics of the five tested models, while Figures 8 and 9 illustrate the new ROP model's predictions against measured data for both wells. The natural heterogeneity of the drilled sequences—comprising limestone, dolomite, sandstone, shale, anhydrite, and marly limestone—is the primary explanation for the observed scatter and outliers in ROP predictions. Rapid vertical variations in lithology, porosity, fracture density, and diagenetic alteration produce localized departures between predicted and measured ROP that no single geomechanical parameter can fully capture. This variability is directly reflected in the wide standard deviations of the ROP data: Well A ranges from 1.9 to 92.7 m/h (mean = 19.6, SD = 10.7 m/h) and Well B from 1 to 43.8 m/h (mean = 9.6, SD = 5.1 m/h). Despite this extreme heterogeneity, the new model achieves R^2 = 0.6568 for Well A and R^2 = 0.6766 for Well B, representing a substantial improvement over the best-performing benchmark formulation (Bourgoyne and Young, R^2 = 0.294 and 0.217 for Wells A and B, respectively). Within lithologically more homogeneous depth intervals, the agreement between predicted and measured ROP is significantly improved, as demonstrated in Figures 8 and 9.

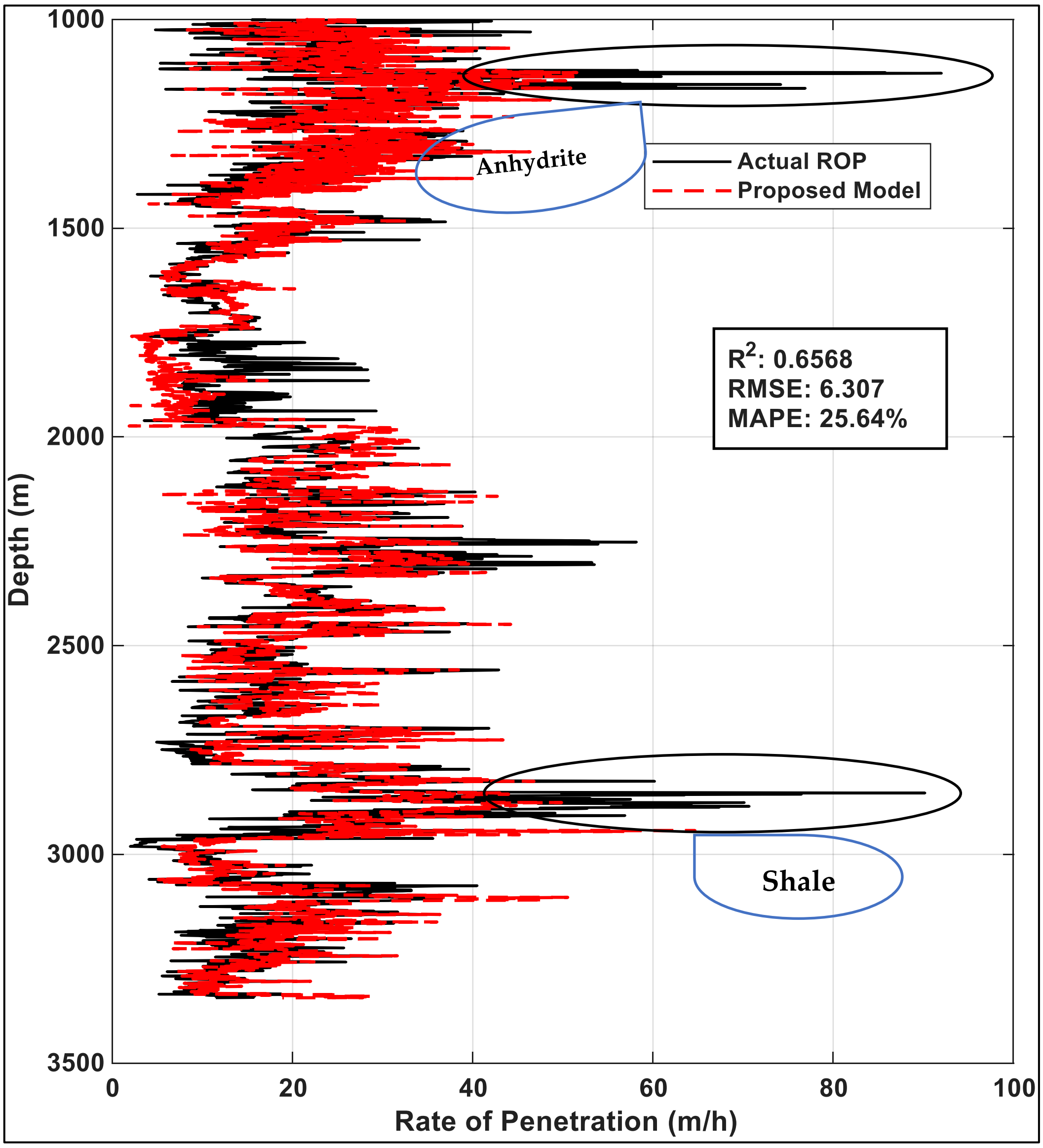

Figure 8. New ROP model performance: measured vs. predicted ROP with depth (Well A–full section).

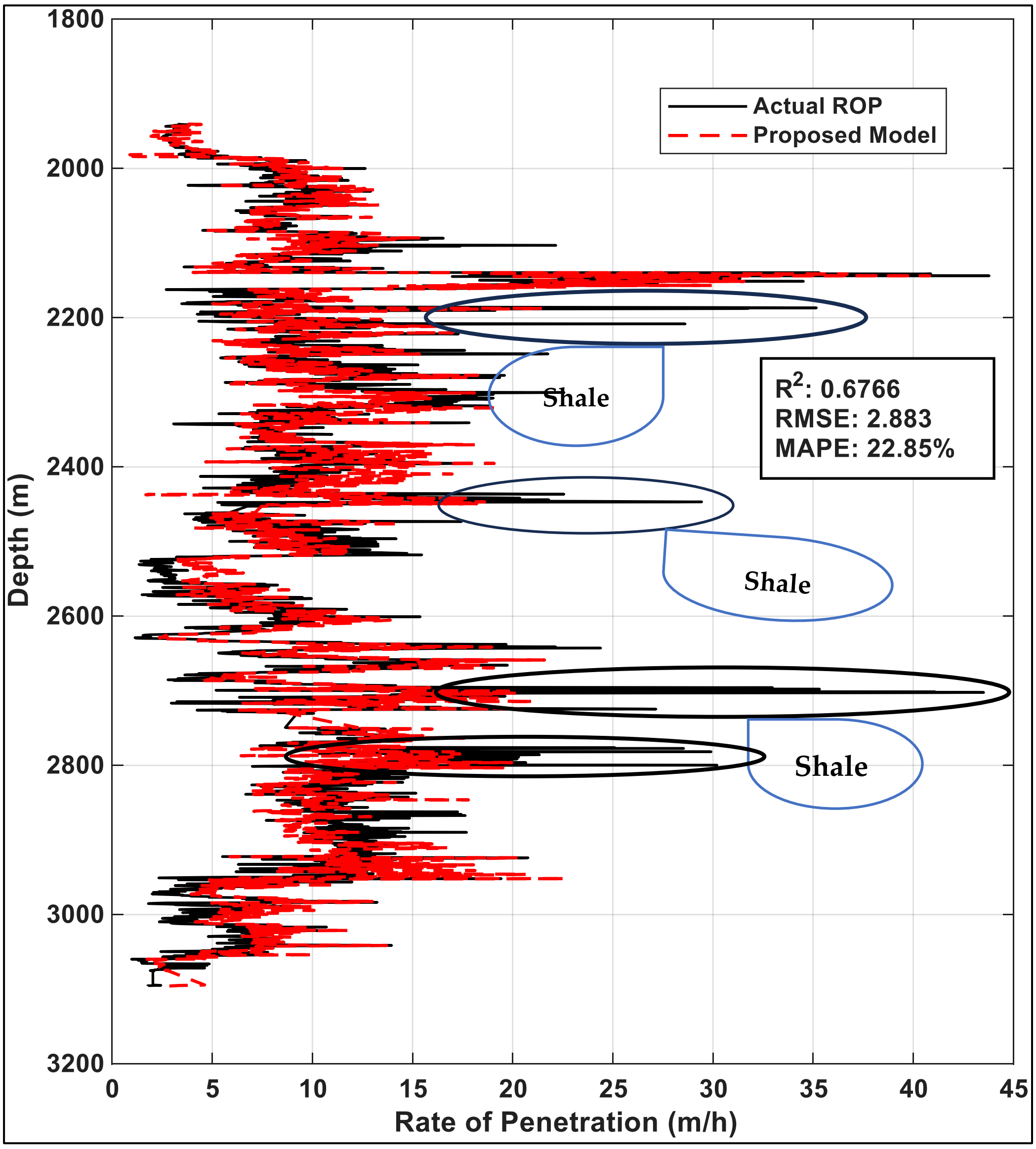

Figure 9. New ROP model performance: measured vs. predicted ROP with depth (Well B)–full section.

Table 7. Performance comparison of ROP models (Well A)–full section.

Model	R^2	RMSE	MAPE%
New model	0.6568	6.307	25.64
Maurer	−3.0023	21.54	87.4
Bingham	0.1808	9.74	41.5
Bourgoyne and Young	0.294	9.04	41
Al-Abduljabbar	0.0644	10.41	43.8

Table 8. Performance comparison of ROP models (Well B)–full section.

Model	R^2	RMSE	MAPE%
New model	0.6766	2.883	22.85
Maurer	−2.3492	9.71	129.7

Table 8. *Cont.*

Model	R^2	RMSE	MAPE%
Bingham	0.0657	5.13	62.2
Bourgoyne and Young	0.217	4.67	56
Al-Abduljabbar	−1.0997	7.69	74.6

For field deployment, the proposed model primarily serves as a robust pre-drill planning tool. Executing the model prior to drilling requires specific offset well wireline logs, namely, DTCO, DTSM, RHOB, PHIT, and GR. These logs provide all the necessary data to pre-calculate the geomechanical profiles, including the dynamic combined modulus (DCM) and overburden pressure (OBP), and to identify the lithology for applying the appropriate functional equation. Furthermore, planned bit specifications (e.g., nozzle diameter, dn) must be defined. While designed for pre-drill optimization, the formulation is highly adaptable to near-real-time applications. Because the mechanical and hydraulic surface parameters (W, N, Torque, SPP) are actively measured at the rig, integrating the model with logging-while-drilling (LWD) acoustic and density data allows for continuous updating of the geomechanical and lithological inputs, thereby enabling dynamic ROP monitoring and re-calibration during active drilling operations.

The significant differences in model coefficients between Wells A and B (Table 9) underscore the necessity of site-specific calibration. This variability is physically expected, as the β parameters absorb localized formation effects (such as cementation, diagenesis, and local stress states) that are not explicitly captured by the primary model inputs, analogous to the field-specific calibration required by all classical ROP models. Because the current framework relies on conventional wireline well logs (DTCO, RHOB), it operates in field deployment primarily as a pre-drill planning and optimization tool calibrated on historical offset well datasets. Regarding operational transferability to new fields, a highly promising direction is real-time Bayesian updating. When drilling a new well equipped with continuous logging-while-drilling (LWD) acoustic and density telemetry, the calibrated coefficient distributions established from historical offset wells (such as Wells A and B) can serve as statistical priors. These priors can then be sequentially refined during drilling using real-time LWD streams, progressively improving ROP predictions without requiring a fully independent calibration dataset beforehand. Furthermore, establishing a dimensionless grouping of the model coefficients is identified as a complementary future generalization pathway to enhance cross-field applicability.

To quantify prediction uncertainty and evaluate residual scatter, residual-based 1 σ (±1 σ) prediction bounds were computed for each evaluated section as the standard deviation of the prediction residuals between the estimated and measured ROP values. For full heterogeneous well sections, residual scattering yielded (±1 σ uncertainty bounds of ±6.302 m/h for Well A and ±2.884 m/h for Well B. Under lithology-specific calibrations, prediction uncertainty reduced substantially across all formations, as detailed in Table 10 (reaching as low as ±0.641 m/h in Well B limestone). Crucially, the virtual mathematical equivalence between the computed RMSE values and the ±1 σ residual bounds across all evaluated sections confirm that the mean prediction residual is virtually zero. This demonstrates negligible systematic prediction bias, indicating no tendency toward systematic over- or under-prediction across any interval. Furthermore, the progressive reduction in uncertainty from unsegregated full-well sections (±6.302 m/h) down to isolated lithological units confirms that residual scattering is driven primarily by unresolved vertical lithological transitions rather than structural error within the model architecture.

Table 9. Model coefficients for the new ROP model (Wells A and B)–full sections.

Coff.	Well A	Well B
β	2.8409	2.1627
β1	−0.1046	−0.1112
β2	−0.2075	0.0765
β3	−0.2034	−0.0606
β4	−0.3017	−0.3155
β5	−0.8700	−0.1579
β6	1.0486	0.3930
β7	−0.1826	−0.2033
β8	0.1848	−0.1420
β9	−0.1055	0.0651

Table 10. Performance metrics of the new ROP model for specific lithological sections.

Formation Type	R^2	RMSE	MAE	MAPE	±1σ (m/h)
Dolomite with some anhydrite and limestone (Well A)	0.8372	2.719	2.008	14.80%	±2.719
Limestone with some shale (Well A)	0.8782	2.407	1.705	9.36%	±2.408
Limestone with some lst. marly (Well B)	0.8239	0.640	0.491	5.71%	±0.641
Sandstone with some limestone and shale (well A)	0.8546	6.205	4.692	13.83%	±6.213
Sandstone with some shale	0.9139	5.045	4.001	11.78%	±5.058

Study Limitations:

The following limitations should be considered when interpreting the results of this study:

(1) The model is validated on two vertical wells from an offshore oil field in the Middle East; broader applicability requires re-calibration and field validation in other geological settings and basins.
(2) The bit wear sub-model was exercised over a limited IADC dull grade range (0 to 1; Wf = 0.83 to 1.0); extension to BG ≥ 4 should be undertaken with caution and additional calibration data.
(3) The DCM/PHIT switching criterion depends on a lithology column derived from offset well data; in new wells without offset data, real-time mud logging or LWD must be used to establish the lithology column for correct model selection.
(4) The model does not incorporate directional drilling effects and is strictly valid for vertical wells; extension to directional and horizontal wells requires additional parameterization.
(5) Uncertainty quantification is currently limited to ±1σ residual bounds; formal Bayesian or bootstrap prediction intervals are identified as future work to provide more comprehensive uncertainty estimates.

3.3. Lithology-Specific Performance

To evaluate the new ROP model's performance in specific lithology types, the model was validated on selected lithological sections for both Wells A and B. These sections were chosen to represent the dominant formation types encountered during drilling, including dolomite, limestone, and sandstone intervals with varying degrees of heterogeneity. By isolating these lithological units, the model's predictive capability could be assessed under wider controlled geological conditions compared to the mixed formations analyzed in the full well sections.

The results demonstrate a significant improvement in predictive performance when the model is applied to individual lithology types. As shown in Table 10, the coefficient of determination (R^2) values range from 0.8239 to 0.9139 across the different sections, compared with 0.6568 to 0.6766 for the full well sections. This enhancement is particularly evident in the reduction of error metrics, with MAPE values decreasing from 22.85–25.64% for full sections to as low as 5.71% for the limestone interval in Well B and 9.36% for limestone in Well A. The dolomite section in Well A achieved an R^2 of 0.8372 with an MAPE of 14.80%, while the sandstone-dominated sections showed the highest R^2 values of 0.8546 and 0.9139, though with slightly higher absolute errors due to greater ROP variability in these formations.

Figures 10–18 illustrate the model's performance across these different lithology types. The depth profile plots show strong visual agreement between the predicted and measured ROP profile, with the model successfully capturing both the magnitude and trend of ROP variations within each lithological unit.

The improvement in model performance when applied to specific lithologies underscores the influence of formation type on ROP behavior and highlights the value of lithology-specific calibration. These lithology-specific results demonstrate that while the new model performs well across heterogeneous sections, its predictive accuracy is maximized when applied to relatively homogeneous lithological units with formation-specific calibration.

3.3.1. Dolomite Section (Well A)

As shown in Table 11 and Figures 10 and 11, the Al-Abduljabbar model achieved the best performance among the existing models in the dolomite section, with an R^2 of 0.7859, RMSE of 3.119 m/h, and MAPE of 15.63%. The Bourgoyne and Young model also performed reasonably well (R^2 = 0.5640, MAPE = 26.08%), while the Bingham and Maurer models exhibited very poor predictive capability with near-zero or negative R^2 values, indicating that these formulations are unsuitable for dolomite formations. In comparison, the new ROP model achieved an R^2 of 0.8372 in this section, outperforming all existing models.

Table 11. Performance comparison of existing ROP models—dolomite (Well A).

Model	R^2	RMSE	MAPE	MAE
New Model	0.8372	2.719	14.80	2.008
Bingham	0.0022165	6.732	42.593	5.3068
Maurer	−0.038336	6.8674	40.052	5.3231
Bourgoyne and Young	0.564	4.4501	26.077	3.3824
Al-Abduljabbar	0.78585	3.1188	15.631	2.2057

3.3.2. Limestone Section (Well A)

In the limestone section of Well A (Table 12, Figures 12 and 13), the Al-AbdulJabbar model again demonstrated the highest accuracy among existing models (R^2 = 0.5275, MAPE = 16.62%), followed by Bourgoyne and Young (R^2 = 0.2553, MAPE = 26.61%). The Maurer model performed particularly poorly in this interval, yielding a negative R^2 of −7.198 and RMSE of 19.745 m/h. The Bingham model also showed negligible predictive power (R^2 = −0.0175). The new model significantly outperformed all existing models in this section, achieving an R^2 of 0.8782 and MAPE of 9.36%.

Table 12. Performance comparison of existing ROP models—limestone (Well A).

Model	R^2	RMSE	MAPE	MAE
New Model	0.8782	2.407	9.36	1.705
Bingham	−0.017516	6.9562	33.545	5.4399
Maurer	−7.1982	19.745	82.656	15.463
Bourgoyne and Young	0.2553	5.951	26.61	4.4853
Al-Abduljabbar	0.52754	4.7401	16.617	3.1393

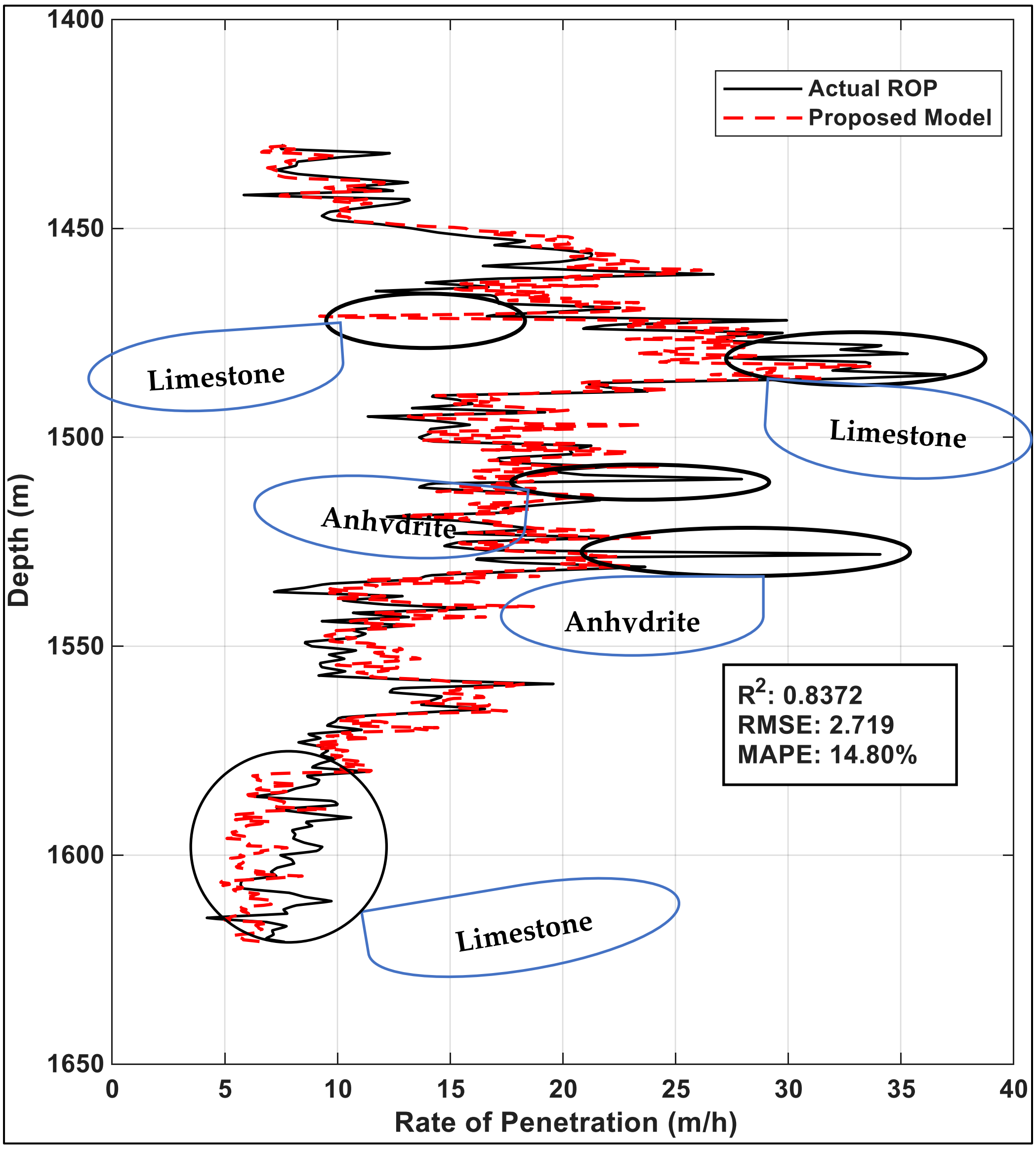

Figure 10. New ROP model: measured vs. predicted ROP with depth—dolomite (Well A).

3.3.3. Limestone Section (Well B)

For the limestone interval in Well B (Table 13, Figures 14 and 15), the Bourgoyne and Young model achieved the highest accuracy among existing models (R^2 = 0.5160, MAPE = 9.84%), followed by Bingham (R^2 = 0.3647, MAPE = 11.79%). The Al-Abduljabbar model showed relatively weaker performance in this interval (R^2 = 0.2505, MAPE = 12.64%), while the Maurer model again exhibited a negative R^2 (−0.7833). The new model achieved an R^2 of 0.8239 and MAPE of 5.71% in this section, representing a substantial improvement over all existing formulations.

Table 13. Performance comparison of existing ROP models—limestone (Well B).

Model	R^2	RMSE	MAPE	MAE
New Model	0.8239	0.640	5.71	0.491
Bingham	0.36467	1.2146	11.786	0.95926
Maurer	−0.78329	2.0349	19.291	1.6828
Bourgoyne and Young	0.51596	1.0602	9.8364	0.834
Al-Abduljabbar	0.25054	1.3192	12.644	1.1041

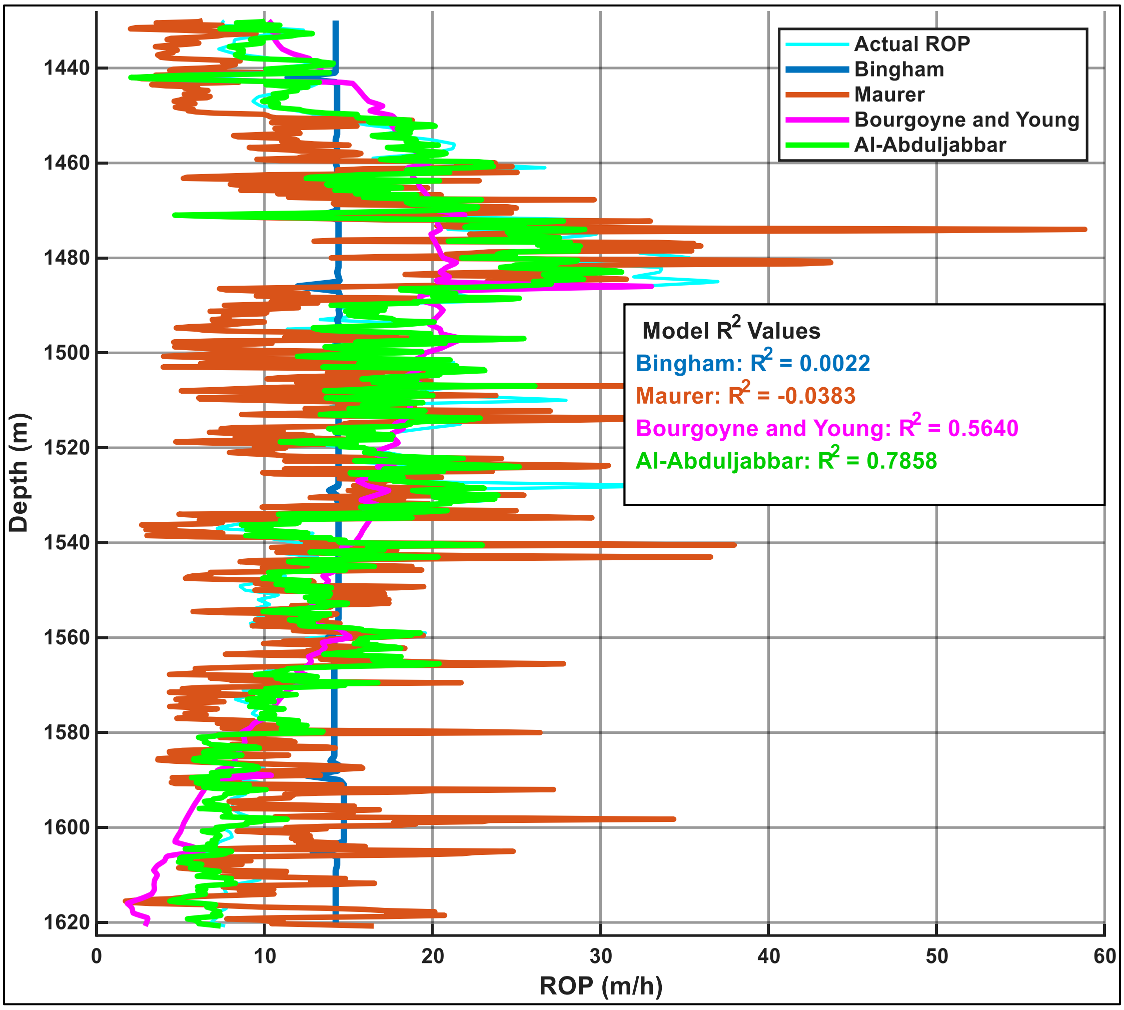

Figure 11. Existing ROP models: measured vs. predicted ROP with depth—dolomite (Well A).

3.3.4. Sandstone Section (Well A)

In the sandstone-dominated interval of Well A (Table 14, Figures 16 and 17), all existing models showed limited predictive capability. The highest R^2 among them was only 0.2391 (Al-Abduljabbar), with MAPE values exceeding 37% for all models. The Maurer model performed worst, with an R^2 of −0.9828 and RMSE of 22.91 m/h. These poor results suggest that existing models struggle to capture complex ROP behavior in heterogeneous sandstone formations containing interbedded shale and limestone. In contrast, the new model achieved an R^2 of 0.8546 and MAPE of 13.83% for the sandstone with some limestone and shale interval, and an R^2 of 0.9139 with MAPE of 11.78% for the sandstone with some shale interval. Figure 18 shows the performance of model for sandstone with some shale.

Table 14. Performance comparison of existing ROP models—sandstone (Well A).

Model	R^2	RMSE	MAPE	MAE
New Model	0.8546	6.205	13.83	4.692
Bingham	0.051917	15.842	41.856	13.487
Maurer	−0.98281	22.91	50.274	18.364
Bourgoyne and Young	0.17111	14.813	37.951	12.366
Al-Abduljabbar	0.23907	14.192	37.729	12.165

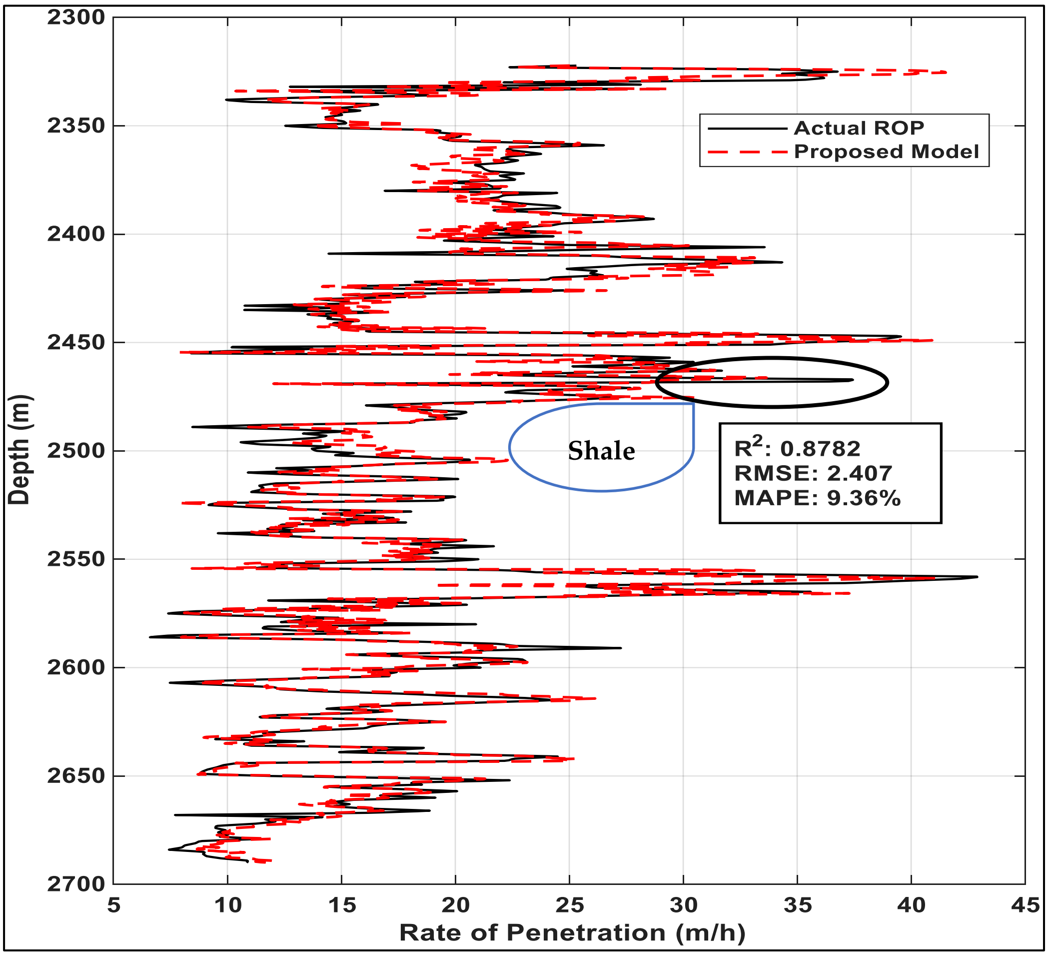

Figure 12. The new ROP model: measured vs. predicted ROP with depth—limestone with some shale (Well A).

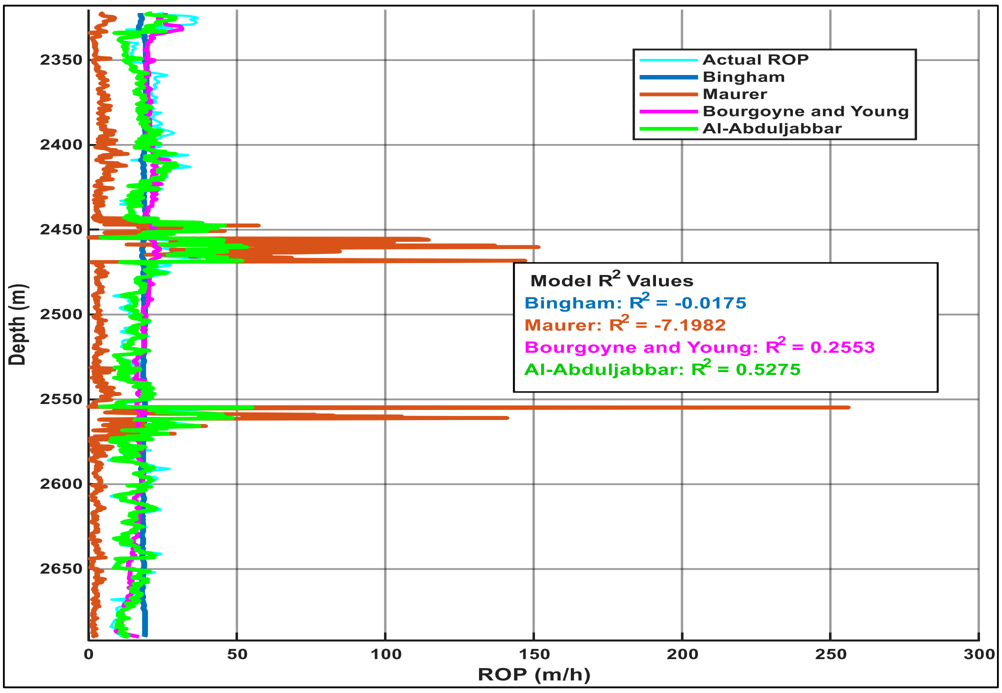

Figure 13. Existing ROP models: measured vs. predicted ROP with depth—limestone (Well A).

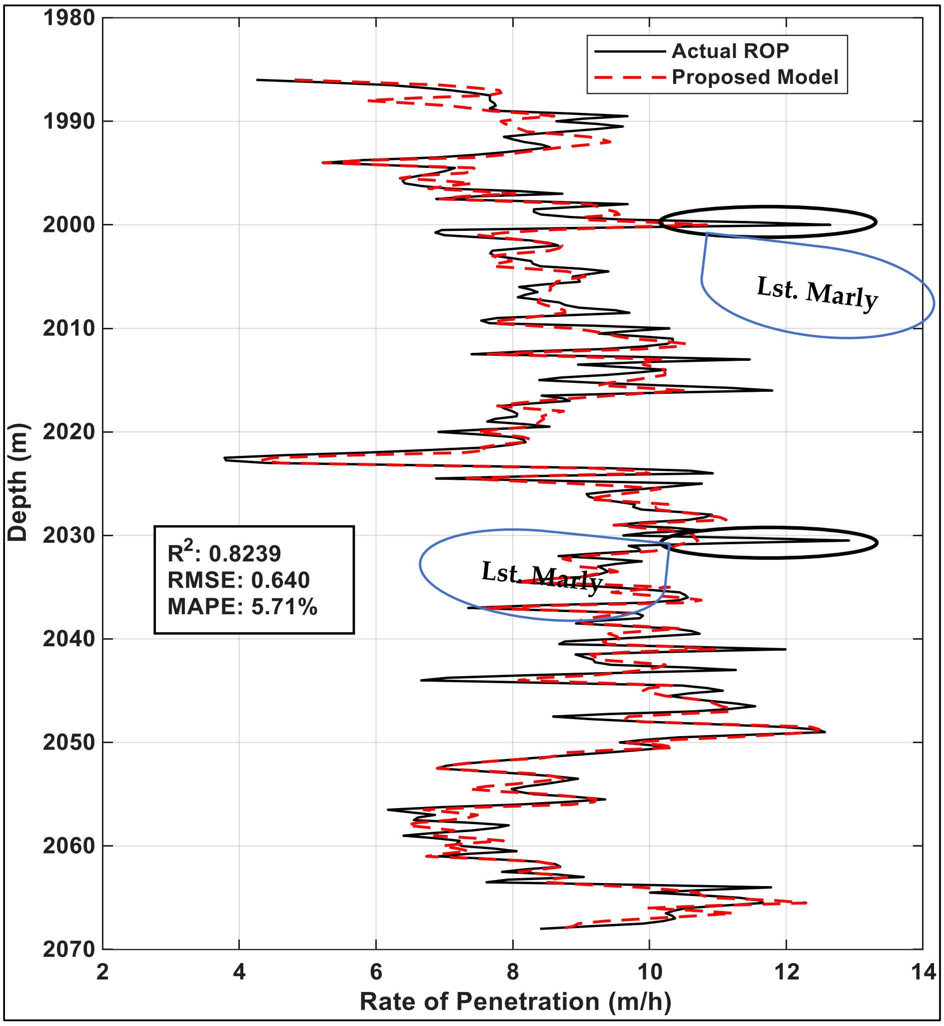

Figure 14. New ROP model: measured vs. predicted ROP with depth—limestone with some lst. marly (Well B).

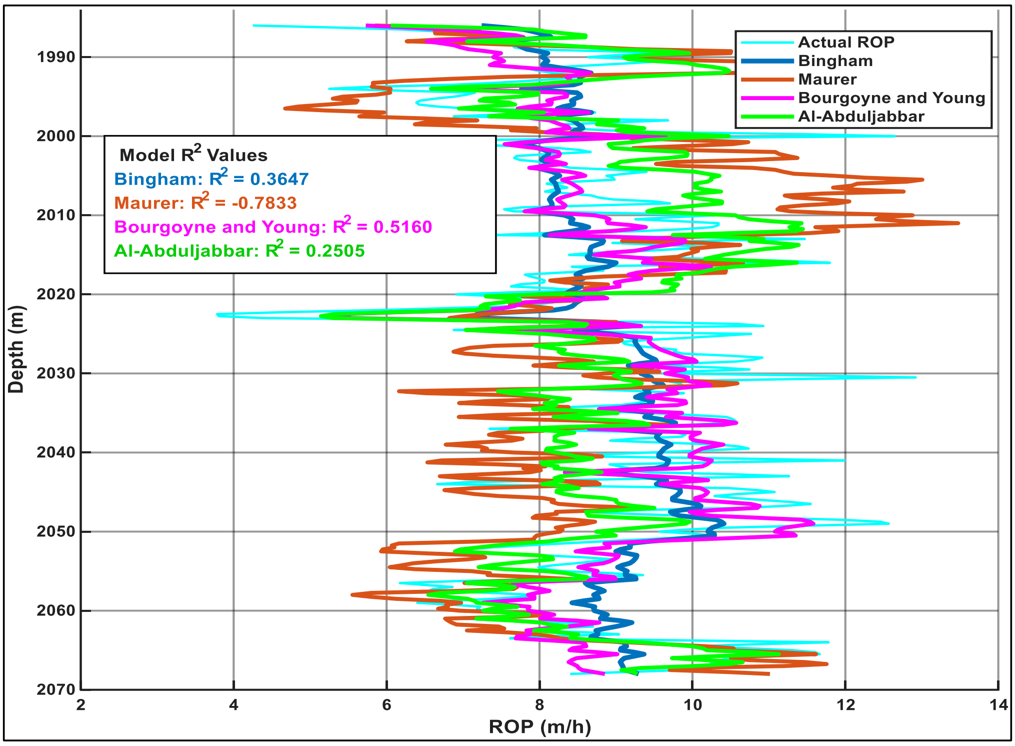

Figure 15. Existing ROP models: measured vs. predicted ROP with depth—limestone (Well B).

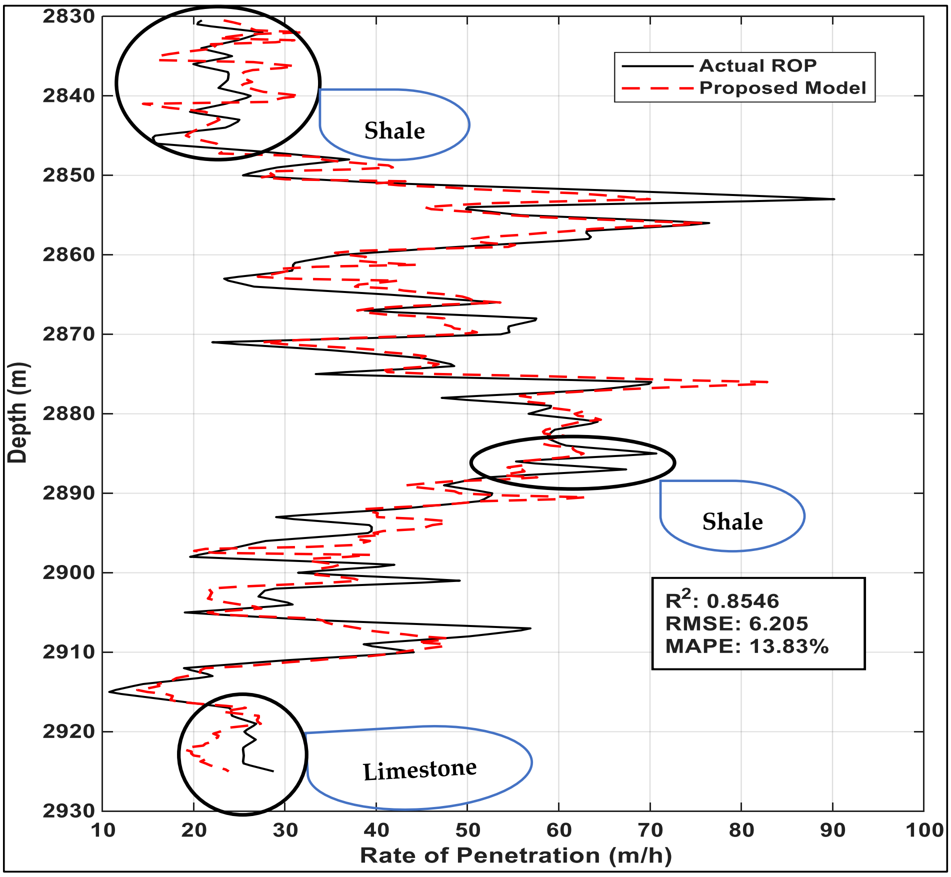

Figure 16. New ROP model: measured vs. predicted ROP with depth—sandstone with some limestone and shale (Well A).

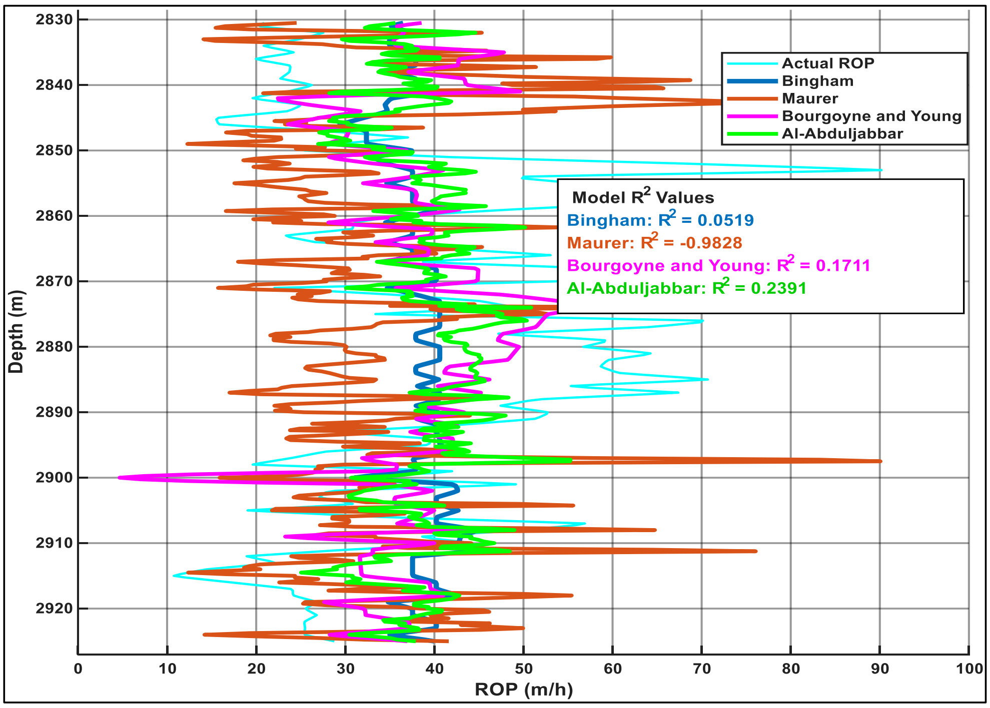

Figure 17. Existing ROP models: measured vs. predicted ROP with depth—sandstone (Well A).

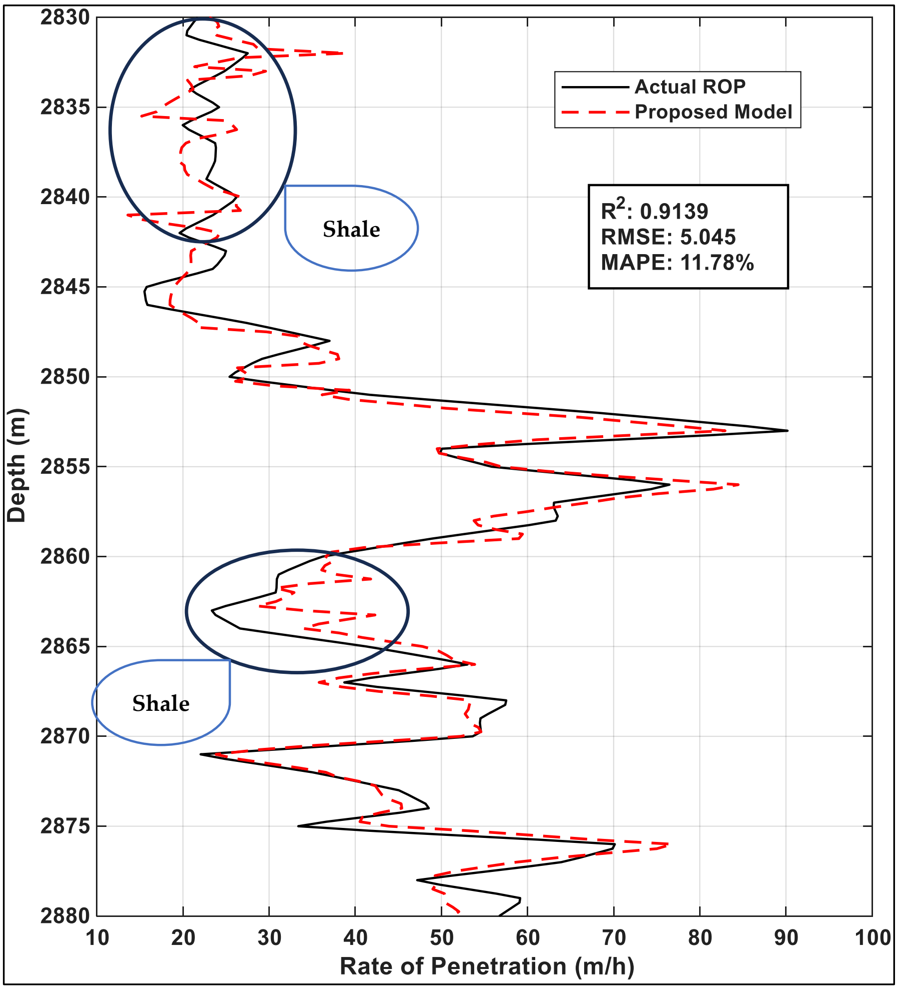

Figure 18. New ROP model: measured vs. predicted ROP with depth—sandstone with some shale (Well A).

4. Conclusions

A novel, physically interpretable Rate of Penetration (ROP) prediction model was developed and validated using drilling data from two vertical wells in a heterogeneous Middle Eastern offshore field. By integrating surface drilling parameters with continuous log-derived geomechanical properties and physically motivated energy parameters, the proposed model demonstrates superior predictive reliability compared to classical formulations. The following main conclusions are drawn.

1. The newly developed model achieves high predictive accuracy across full heterogeneous well sections, substantially outperforming the best-performing classical benchmark formulations. Furthermore, when applied to individual lithological intervals, the model's accuracy improves significantly, proving its robustness and adaptability in complex geological settings.
2. Integrating log-derived geomechanical properties and physically motivated energy parameters provides a significant and measurable improvement in prediction accuracy over models relying solely on surface drilling data. This validates the principle that embedding physical drilling mechanics into the feature space is essential for capturing complex rock-bit interactions in heterogeneous formations.
3. Lithology-specific calibration is essential for minimizing prediction errors across diverse geological sequences. The ability to adapt the model's coefficients to specific rock types substantially reduces overall error margins, demonstrating that a single, static coefficient set cannot adequately represent the varying drilling dynamics of interbedded formations.
4. Traditional fixed-exponent models fail entirely in highly heterogeneous sequences, often yielding physically impossible negative prediction accuracies, particularly in sandstone intervals. In contrast, the proposed model maintains high accuracy across all tested lithologies by dynamically adapting to local rock properties. Ultimately, this proves that reliable ROP prediction requires the simultaneous integration of geomechanical and energy-based parameters—a level of adaptability that cannot be achieved through simple coefficient tuning of existing fixed-structure models.
5. Because the present study utilizes conventional wireline logs, the model currently serves in field operations primarily as a pre-drill planning and parameter optimization tool calibrated on historical offset well data. However, from a practical deployment perspective, the model demonstrates strong potential for real-time implementation when integrated with LWD acoustic and density telemetry. Feeding real-time LWD streams directly into the formation characterization workflow allows the model to dynamically predict and optimize ROP ahead of the bit. Furthermore, the model's reliance on log-derived parameters computed by standard petrophysical software inherently applies quality control and smoothing filters, which effectively moderate the model's sensitivity to raw surface sensor noise during field deployment.
6. While validated as a proof of concept using conventional wireline logs in two vertical wells within a single Middle Eastern offshore field, future work must extend the model's applicability to directional and horizontal wells and incorporate PDC-specific cutter geometry extensions. Additionally, establishing dimensionless grouping of the model coefficients and exploring Bayesian updating—where historical offset well calibrations serve as priors that are progressively refined using real-time LWD telemetry—will enhance cross-field transferability and pave the way for fully autonomous, real-time drilling optimization systems.

Author Contributions: Conceptualization, M.A.K. and A.S.A.; methodology, M.A.K., M.N.J.A., and A.S.A.; software, M.A.K. and A.S.A.; validation, M.A.K.; formal analysis, M.A.K.; investigation,

M.A.K.; resources, M.A.K.; data curation, M.A.K. and A.S.A.; writing—original draft preparation, M.A.K. and A.S.A.; writing—review and editing, M.A.K. and M.N.J.A.; visualization, M.A.K.; supervision, M.A.K.; project administration, M.A.K.; funding acquisition, M.A.K. All authors have read and agreed to the published version of the manuscript.

Funding: This research received no external funding.

Institutional Review Board Statement: Not applicable.

Informed Consent Statement: Not applicable.

Data Availability Statement: All data supporting the findings of this work are presented within the article. For any further inquiries, please contact the corresponding author.

Acknowledgments: This work was supported by the Ongoing Research Funding program (ORF-2026-1616), King Saud University, Riyadh, Saudi Arabia. The authors would like to express their gratitude to the Department of Petroleum and Natural Gas Engineering at King Saud University for its assistance and support through this study.

Conflicts of Interest: The authors declare no conflicts of interest.

Abbreviations

The following abbreviations are used in this manuscript:

BG	Cumulative bit wear (IADC scale 0–8)
BI	Brittleness index
CCS	Confined compressive strength, psi
DCM	Dynamic combined modulus, Mpsi
Differ. Press	Differential pressure, Psi
dn	Nozzle diameter, in
DRES	Deep resistivity log, ohm.m
DTCO	Compressional slowness, us/ft
DTSM	Shear slowness, us/ft
ECD	Equivalent circulating density, Ibm/gal
EDYN	Dynamic Young's modulus, Mpsi
FA	Friction angle, degree
GDYN	Dynamic shear modulus, (Mpsi)
GR	Gamma ray
hc	Bit wear calibration coefficient
HHP	Hydraulic horsepower, psi
KDYN	Dynamic bulk modulus, Mpsi
LMF	Log measured from (drill floor)
MAE	Mean absolute error
MAPE	Mean absolute percentage error
N	Rotary speed, rpm
OBP	Over burden pressure, psi
PEF	Photoelectric factor
PHIT	Total porosity
PP	Pore pressure, psi
PR	Poisons ratio
R^2	Coefficient of determination
RHOB	Bulk density, g/cc
RMSE	Root mean square error
SHMINP	Minimum horizontal stress, psi
SHMMAX	Maximum horizontal stress, psi
SPP	Standpipe pressure, psi
T	Surface torque, Ibf-ft

TNPH	Thermal neutron porosity
TWC	Thick wall cylinder, psi
UCS	Unconfined compressive strength
VCL	Clay volume
W	Weight on bit, ton
Wf	Bit wear function (fractional effectiveness)
ΔBG	Incremental bit wear per depth step

References

1. Gan, C.; Cao, W.; Wu, M.; Liu, K.-Z.; Chen, X.; Hu, Y.; Ning, F. Two-level intelligent modeling method for the rate of penetration in complex geological drilling process. *Appl. Soft Comput.* **2019**, *80*, 592–602. [CrossRef]
2. Gan, C.; Cao, W.-H.; Wu, M.; Chen, X.; Hu, Y.-L.; Liu, K.-Z.; Wang, F.-W.; Zhang, S.-B. Prediction of drilling rate of penetration (ROP) using hybrid support vector regression: A case study on the Shennongjia area, Central China. *J. Pet. Sci. Eng.* **2019**, *181*, 106200. [CrossRef]
3. Gan, C.; Cao, W.-H.; Liu, K.-Z.; Wu, M.; Wang, F.-W.; Zhang, S.-B. A New Hybrid Bat Algorithm and its Application to the ROP Optimization in Drilling Processes. *IEEE Trans. Ind. Inform.* **2020**, *16*, 7338–7348. [CrossRef]
4. Zhou, Y.; Chen, X.; Zhao, H.; Wu, M.; Cao, W.; Zhang, Y.; Liu, H. A novel rate of penetration prediction model with identified condition for the complex geological drilling process. *J. Process Control.* **2021**, *100*, 30–40. [CrossRef]
5. Li, Y.; Cao, W.; Hu, W.; Wu, M. Detection of downhole incidents for complex geological drilling processes using amplitude change detection and dynamic time warping. *J. Process Control.* **2021**, *102*, 44–53. [CrossRef]
6. Zhang, Z.; Lai, X.; Wu, M.; Chen, L.; Lu, C.; Du, S. Fault diagnosis based on feature clustering of time series data for loss and kick of drilling process. *J. Process Control.* **2021**, *102*, 24–33. [CrossRef]
7. Faronov, M.V.; Polushin, I.G. Observer-based control of vertical penetration rate in rotary drilling systems. *J. Process Control.* **2021**, *106*, 29–43. [CrossRef]
8. Bourgoyne, A.T.; Millheim, K.K.; Chenevert, M.E.; Young, F.S. *Applied Drilling Engineering*; Society of Petroleum Engineers Textbook Series; Society of Petroleum Engineers: Richardson, TX, USA, 1986.
9. Yi, P.; Kumar, A.; Samuel, R. Realtime Rate of Penetration Optimization Using the Shuffled Frog Leaping Algorithm. *J. Energy Resour. Technol.* **2014**, *137*, 032902. [CrossRef]
10. Ghasemloonia, A.; Rideout, D.G.; Butt, S.D. Vibration Analysis of a Drillstring in Vibration-Assisted Rotary Drilling: Finite Element Modeling With Analytical Validation. *J. Energy Resour. Technol.* **2013**, *135*, 032902. [CrossRef]
11. Kamel, M.A.; Elkatatny, S.; Mysorewala, M.F.; Al-Majed, A.; Elshafei, M. Adaptive and Real-Time Optimal Control of Stick–Slip and Bit Wear in Autonomous Rotary Steerable Drilling. *J. Energy Resour. Technol.* **2017**, *140*, 032908. [CrossRef]
12. Akgun, F. How to Etimate the Maximum Achievable Drilling Rate without Jeopardizing Safety. In Proceedings of the Abu Dhabi International Petroleum Exhibition and Conference, Abu Dhabi, United Arab Emirates, 13–16 October 2002. [CrossRef]
13. Sobhi, I.; Dobbi, A.; Hachana, O. Prediction and analysis of penetration rate in drilling operation using deterministic and metaheuristic optimization methods. *J. Pet. Explor. Prod. Technol.* **2022**, *12*, 1341–1352. [CrossRef]
14. Cheniany, A.; Hasan, K.S.; Shahriar, K.; Hamidi, J.K. An estimation of the penetration rate of rotary drills using the Specific Rock Mass Drillability index. *Int. J. Min. Sci. Technol.* **2012**, *22*, 187–193. [CrossRef]
15. Nascimento, A.; Elmgerbi, A.; Roohi, A.; Prohaska, M.; Thonhauser, G.; Gonçalves, J.L.; Mathias, M.H. Reverse Engineering: A New Well Monitoring and Analysis Methodology Approaching Playing-Back Drill-Rate Tests in Real-Time for Drilling Optimization. *J. Energy Resour. Technol.* **2016**, *139*, 012902. [CrossRef]
16. Youcefi, M.R.; Hadjadj, A.; Bentriou, A.; Boukredera, F.S. Rate of penetration modeling using hybridization extreme learning machine and whale optimization algorithm. *Earth Sci. Inform.* **2020**, *13*, 1351–1368. [CrossRef]
17. Graham, J.W.; Muench, N.L. Analytical Determination of Optimum Bit Weight and Rotary Speed Combinations. In Proceedings of the Fall Meeting of the Society of Petroleum Engineers of AIME, Dallas, TX, USA, 4–7 October 1959. [CrossRef]
18. Maurer, W.C. The "Perfect—Cleaning" Theory of Rotary Drilling. *J. Pet. Technol.* **1962**, *14*, 1270–1274. [CrossRef]
19. Bingham, M.G. *A New Approach to Interpreting—Rock Drillability*; Technical Manual Reprint; Petroleum Publishing Company: Tulsa, OK, USA, 1965.
20. Eckel, J.R. Microbit Studies of the Effect of Fluid Properties and Hydraulics on Drilling Rate. *J. Pet. Technol.* **1967**, *19*, 541–546. [CrossRef]
21. Bourgoyne, A.J., Jr.; Young, F.S., Jr. A Multiple Regression Approach to Optimal Drilling and Abnormal Pressure Detection. *Soc. Pet. Eng. J.* **1974**, *14*, 371–384. [CrossRef]
22. Eren, T.; Ozbayoglu, M.E. Real-Time Drilling Rate Of Penetration Performance Monitoring. In Proceedings of the Offshore Mediterranean Conference and Exhibition, Ravenna, Italy, 23–25 March 2011.

23. Warren, T.M. Penetration-Rate Performance of Roller-Cone Bits. *SPE Drill. Eng.* **1987**, *2*, 9–18. [CrossRef]
24. Maidla, E.E.; Ohara, S. Field Verification of Drilling Models and Computerized Selection off Drill Bit, WOB, and Drillstring Rotation. *SPE Drill. Eng.* **1991**, *6*, 189–195. [CrossRef]
25. Hareland, G.; Rampersad, P.R. Drag—Bit Model Including Wear. In Proceedings of the SPE Latin America/Caribbean Petroleum Engineering Conference, Buenos Aires, Argentina, 27–29 April 1994. [CrossRef]
26. Motahhari, H.; Hareland, G.; James, J. Improved Drilling Efficiency Technique Using Integrated PDM and PDC Bit Parameters. *J. Can. Pet. Technol.* **2010**, *49*, 45–52. [CrossRef]
27. Hareland, G.; Wu, A.; Rashidi, B. A Drilling Rate Model for Roller Cone Bits and Its Application. In Proceedings of the International Oil and Gas Conference and Exhibition in China, Beijing, China, 8–10 June 2010. [CrossRef]
28. Deng, Y.; Chen, M.; Jin, Y.; Zhang, Y.; Zou, D.; Lu, Y. Theoretical and experimental study on the penetration rate for roller cone bits based on the rock dynamic strength and drilling parameters. *J. Nat. Gas. Sci. Eng.* **2016**, *36*, 117–123. [CrossRef]
29. Al-AbdulJabbar, A.; Elkatatny, S.; Mahmoud, M.; Abdelgawad, K.; Al-Majed, A. A Robust Rate of Penetration Model for Carbonate Formation. *J. Energy Resour. Technol.* **2018**, *141*, 042903. [CrossRef]
30. Soares, C.; Daigle, H.; Gray, K. Evaluation of PDC bit ROP models and the effect of rock strength on model coefficients. *J. Nat. Gas. Sci. Eng.* **2016**, *34*, 1225–1236. [CrossRef]
31. Atashnezhad, A.; Akhtarmanesh, S.; Sleeper, S.; Hareland, G. Rate of Penetration (ROP) Model for PDC Drill Bits based on Cutter Rock Interaction. In Proceedings of the 54th U.S. Rock Mechanics/Geomechanics Symposium, Virtual, 28 June–1 July 2020.
32. Akhtarmanesh, S.; Atashnezhad, A.; Hareland, G.; Al Dushaishi, M. ROP Model for PDC Bits in Geothermal Drilling. In Proceedings of the 55th U.S. Rock Mechanics/Geomechanics Symposium, Virtual, 18–25 June 2021.
33. Mayibeki, D.N. Novel Rate of Penetration (ROP) Model for Hard Rock Drilling with Application to Geothermal Drilling. Ph.D. Thesis, Oklahoma State University, Stillwater, OK, USA, 2025; p. 32120845. Available online: https://www.proquest.com/dissertations-theses/novel-rate-penetration-rop-model-hard-rock/docview/3251650821/se-2?accountid=44936 (accessed on 18 July 2026).
34. Jahanbakhshi, R.; Keshavarzi, R.; Jafarnezhad, A. Real-time Prediction of Rate of Penetration During Drilling Operation In Oil And Gas Wells. In Proceedings of the 46th U.S. Rock Mechanics/Geomechanics Symposium, Chicago, IL, USA, 24–27 June 2012.
35. Ahmed, O.S.; Adeniran, A.A.; Samsuri, A. Computational intelligence based prediction of drilling rate of penetration: A comparative study. *J. Pet. Sci. Eng.* **2019**, *172*, 1–12. [CrossRef]
36. Delavar, M.R.; Ramezanzadeh, A.; Tokhmechi, B. An investigation into the effect of geomechanical properties of reservoir rock on drilling parameters—A case study. *Arab. J. Geosci.* **2021**, *14*, 1763. [CrossRef]
37. Behboud, M.M.; Ramezanzadeh, A.; Tokhmechi, B.; Mehrad, M.; Davoodi, S. Estimation of geomechanical rock characteristics from specific energy data using combination of wavelet transform with ANFIS-PSO algorithm. *J. Pet. Explor. Prod. Technol.* **2023**, *13*, 1715–1740. [CrossRef]
38. Delavar, M.R.; Ramezanzadeh, A. Machine learning classification approaches to optimize ROP and TOB using drilling and geomechanical parameters in a carbonate reservoir. *J. Pet. Explor. Prod. Technol.* **2024**, *14*, 1–26. [CrossRef]
39. Saad, A.; Taman, A.; Reda, D.; Yehia, T.; Keshinro, O.; Meehan, N.; Okoroafor, E.R. Enhancing Geothermal Drilling Performance: Predicting Rate of Penetration with Machine Learning Utilizing Geomechanical and Petrophysical Data. In Proceedings of the SPE Offshore Europe Conference & Exhibition, Aberdeen, UK, 2–5 September 2025. [CrossRef]
40. Cunningham, R.; Eenink, J. Laboratory Study of Effect of Overburden, Formation and Mud Column Pressures on Drilling Rate of Permeable Formations. *Trans. AIME* **1959**, *217*, 9–17. [CrossRef]
41. Galle, E.M.; Woods, H.B. Best Constant Weight and Rotary Speed for rotary Rock Bits. *Drill. Prod. Pract.* **1963**.
42. Warren, T.M. Drilling Model for Soft-Formation Bits. *J. Pet. Technol.* **1981**, *33*, 963–970. [CrossRef]
43. Walker, B.H.; Black, A.D.; Klauber, W.P.; Little, T.; Khodaverdian, M. Roller-Bit Penetration Rate Response as a Function of Rock Properties and Well Depth. In Proceedings of the SPE Annual Technical Conference and Exhibition, New Orleans, LA, USA, 5–8 October 1986. [CrossRef]
44. Winters, W.J.; Warren, T.M.; Onyia, E.C. Roller Bit Model with Rock Ductility and Cone Offset. In Proceedings of the SPE Annual Technical Conference and Exhibition, Dallas, TX, USA, 27–30 September 1987. [CrossRef]
45. Hareland, G.; Hoberock, L.L. Use of Drilling Parameters to Predict In-Situ Stress Bounds. In Proceedings of the SPE/IADC Drilling Conference, Amsterdam, The Netherlands, 23–25 February 1993. [CrossRef]
46. Hareland, G.; Wu, A.; Rashidi, B.; James, J. A New Drilling Rate Model for Tricone Bits and Its Application to Predict Rock Compressive Strength. In Proceedings of the 44th US Rock Mechanics Symposium and 5th U.S.-Canada Rock Mechanics Symposium, Salt Lake City, UT, USA, 27–30 June 2010.
47. Mazen, A.Z.; Rahmanian, N.; Mujtaba, I.; Hassanpour, A. Prediction of Penetration Rate for PDC Bits Using Indices of Rock Drillability, Cuttings Removal, and Bit Wear. *SPE Drill. Complet.* **2021**, *36*, 320–337. [CrossRef]
48. Sauki, A.; Khamaruddin, P.N.F.M.; Irawan, S.; Kinif, I.; Ridha, S.; Ali, S.A.; Ali, M.A. Development of a modified Bourgoyne and Young model for predicting drilling rate. *J. Pet. Sci. Eng.* **2021**, *205*, 108994. [CrossRef]

49. Alhalboosi, A.S.; AlAwad, M.N.J.; Altawati, F.S.; Khamis, M.A.; Almobarky, M.A. Optimal Geomechanical Parameter Selection for Enhanced ROP Modeling: A Systematic Field-Based Comparative Study. *Processes* **2026**, *14*, 1646. [CrossRef]
50. Allawi, R.H.; Al-Mudhafar, W.J.; Thanh, H.V.; Sepehrnoori, K. Novel semi-analytical model for estimating unconfined compressive strength in sandstone reservoirs: Implications for CO_2 sequestration. *Next Energy* **2026**, *11*, 100562. [CrossRef]